July 2006

Influence of Non-Stoichiometry on the Structure and Properties of $Ba(Zn_{1/3}Nb_{2/3})O_3$ Microwave Dielectrics: II. Compositional Variations in Pure BZN

Hui Wu
University of Pennsylvania

Peter K. Davies
University of Pennsylvania, davies@lrsm.upenn.edu

Influence of Non-Stoichiometry on the Structure and Properties of $Ba(Zn_{1/3}Nb_{2/3})O_3$ Microwave Dielectrics: II. Compositional Variations in Pure BZN

Abstract

The formation of non-stoichiometric cubic perovskite solid solutions based on $BaZn_{1/3}Nb_{2/3}O_3$ (BZN) was examined along 10 different directions in the $BaO–ZnO–Nb_2O_5$ ternary system. Limited ranges of non-stoichiometry were observed along several pseudo-binaries and the BZN structure can accommodate a variety of different types of defects. Although the deviations from stoichiometry are quite small, typically ~1 mole%, they induce large changes in the extent and stability of the 1:2 B-site ordering, the sintering and microstructure, and the dielectric loss properties. The highest $Q \times fs$ (~110 000 at 8 GHz) in the system, which coincide with the highest degree of order, were located in two regions along the BZN–$Ba_5Nb_4O_{15}$ and BZN–$BaNb_2O_6$ lines. The results of this study provide an explanation for the large variations in crystal structure and $Q \times fs$ previously reported for BZN and other related systems (e.g., $Ba(Zn_{1/3}Ta_{2/3})O_3$), and demonstrate that non-stoichiometric starting compositions provide a route to the highest Q values.

journal

J. Am. Ceram. Soc., 89 [7] 2250–2263 (2006)
DOI: 10.1111/j.1551-2916.2006.01008.x

Influence of Non-Stoichiometry on the Structure and Properties of $Ba(Zn_{1/3}Nb_{2/3})O_3$ Microwave Dielectrics: II. Compositional Variations in Pure BZN

Hui Wu and Peter K. Davies†

Department of Materials Science and Engineering, University of Pennsylvania, Philadelphia, Pennsylvania 19104-6272

The formation of non-stoichiometric cubic perovskite solid solutions based on $BaZn_{1/3}Nb_{2/3}O_3$ (BZN) was examined along 10 different directions in the $BaO–ZnO–Nb_2O_5$ ternary system. Limited ranges of non-stoichiometry were observed along several pseudo-binaries and the BZN structure can accommodate a variety of different types of defects. Although the deviations from stoichiometry are quite small, typically ~1 mole%, they induce large changes in the extent and stability of the 1:2 B-site ordering, the sintering and microstructure, and the dielectric loss properties. The highest $Q \times f$s (~110 000 at 8 GHz) in the system, which coincide with the highest degree of order, were located in two regions along the BZN–$Ba_5Nb_4O_{15}$ and BZN–$BaNb_2O_6$ lines. The results of this study provide an explanation for the large variations in crystal structure and $Q \times f$s previously reported for BZN and other related systems (e.g., $Ba(Zn_{1/3}Ta_{2/3})O_3$), and demonstrate that non-stoichiometric starting compositions provide a route to the highest Q values.

I. Introduction

SMALL deviations in the stoichiometry of $Ba(Zn_{1/3}Nb_{2/3})O_3$ (BZN) and other related microwave perovskites have a profound effect on their ordering, sintering, and dielectric properties.[1–5] In a previous paper, the formation of small concentrations (<1%) of zinc vacancies on the B sites, introduced through the substitution of $Ba_3W_2O_9$ (BW) into BZN, was shown to enhance the relative stability of the 1:2 order, accelerate the kinetics of the ordering and domain-coarsening process, and allow the c/a lattice distortion to approach its maximum value.[1] The $Ba_3W_2O_9$ additive also lowered the sintering temperature of BZN, and dense ceramics with $Q \times f$ values (118 500 at 8 GHz) that rival those of the "super Q" tantalates could be prepared at 1390°C. This paper examines the formation of substituent-free, non-stoichiometric, vacancy-containing solid solutions of BZN in the $BaO–ZnO–Nb_2O_5$ system.

The cubic perovskite structure is well known to accommodate large degrees of non-stoichiometry and vacancy formation on the A-site and anion positions. While the B sites readily accept multiple cations, the degree of vacancy formation on this position is limited to concentrations less than 2%.[6] Larger concentrations of B-site vacancies alter the stacking of the AO3 layers and result in the formation of so-called hexagonal perovskite structures where the vacancies are often ordered in the resultant layers of face-shared octahedra. For $Ba(Zn_{1/3}Ta_{2/3})O_3$ (BZT), deviations from stoichiometry induced by the volatilization of ZnO have been reported to promote the growth of the ordered domains,[7] increase the extent of cation ordering[8] and the c/a lattice distortion,[9] and improve the dielectric loss properties.[10] Beneficial effects of cation deficiency on the losses have also been observed in other 1:2 complex perovskites such as $BaMg_{1/3}Ta_{2/3}O_3$ (BMT)[2,3] and $BaMg_{1/3}Nb_{2/3}O_3$ (BMN).[4]

However, a variety of different mechanisms and even conflicting results have appeared in the literature for the effect of the nonstoichiometry on the cation ordering. For BZT, it was proposed that the loss of Zn and associated reduction in the Zn:Nb ratio increased the extent of ordering and the c/a distortion due to the partial replacement of Zn by the Ba A-site cations.[9] Recently, the formation of zinc vacancies from the loss of ZnO was reported to enhance the cation diffusion and domain growth, and a higher extent of cation order was observed in free BZT powders compared with a pellet.[7,8] Support for the formation of Zn-deficient BZT phases was obtained from high-resolution neutron and X-ray scattering, and two BZT phases with slightly different cell parameters and c/a ratios were observed. Refinements of the occupancies of these phases led to a best fit where one was stoichiometric and the other contained Zn vacancies. In contrast to the results for BZT, in $BaZn_{1/3}Nb_{2/3}O_3$ and $BaNi_{1/3}Nb_{2/3}O_3$ (BNN), the formation of defects on the B sites from the loss of ZnO or NiO was reported to induce cation disorder.[5] This observation was explained in terms of vacancy formation during the partial melting of the phases, which was claimed to increase in the degree of anti-site disorder.[5]

A variety of conflicting reports have also appeared on the effect of non-stoichiometry on the grain growth and densification of these systems. For BZT,[10] volatilization of ZnO was reported to induce secondary phase formation and inhibit densification. Volatilization was prevented and the density improved when the samples were muffled in ZnO, although the resultant $Q \times f$ value decreased. In contrast, small amounts of MgO deficiency in BMN were found to increase the density,[4] while excess MgO retarded the grain growth and densification.[2]

Conflicting data have also appeared on the effect of A-site non-stoichiometry on the microstructure and densification. In BMT, a deficiency of BaO was shown to increase the grain size, density, and cation ordering due to the presence of a Mg-rich liquid phase and/or the A-site vacancies.[3] However, no evidence of liquid-phase sintering was found in a different study of BaO-deficient BMT where the samples were prepared from $(MgCO_3)_4 \cdot Mg(OH)_2 \cdot 5H_2O$ instead of MgO.[2] For BaO-excess BNN, abnormal grain growth led to poor densities,[11] while a uniform grain size was observed in BaO-excess BMT.[2] These few examples illustrate the diverse range of conflicting observations that have been made on these systems and highlight the difficulties that can be encountered in their processing.

Extensive deviations from stoichiometry, for example through excessive volatilization of ZnO, cause the formation of secondary phases. The majority of studies have focused on BZT (and

T. Vanderah—contributing editor

Manuscript No. 21120. Received November 4, 2005; approved February 8, 2006.
This work was financially supported by the National Science Foundation through award DMR 02-13489 and made use of the MRSEC shared experimental facilities supported by the National Science Foundation through award DMR05-20020.
†Author to whom correspondence should be addressed. e-mail: davies@seas.upenn.edu

BZN) and again there has been little consensus in the literature on their identity or their effect on Q. Most investigations assigned the impurities to a variety of binary barium tantalates (or niobates) that include, but are not limited to, $Ba_3Ta_2O_8$, $Ba_5Ta_4O_{15}$, and $BaTa_2O_6$; almost all of these secondary phases were believed to reduce Q.[12–16] Recently, a Zn-deficient ternary phase, $Ba_8ZnTa_6O_{24}$, whose major diffraction peaks are close to those of the various binary barium tantalates, was confirmed to be the primary impurity in ZnO-deficient BZT.[17,18] This phase, which has a closely related hexagonal perovskite structure, exhibits excellent sintering characteristics and very good microwave properties, $\varepsilon \sim 32.2$, $Q \times f \sim 62\,000$ at 8.9 GHz.[17]

The extreme diversity in the observation and interpretation of the effect of non-stoichiometry, particularly cation vacancy formation, on the structure, sintering, and Q values of BZT and other microwave perovskites, prompted this investigation of the range of nonstoichiometry in BZN and its effect on the cation order, sintering, and dielectric loss properties. The study involved examination of the potential formation of non-stoichiometric BZN solid solutions along 10 pseudo-binary directions in the BaO–ZnO–Nb_2O_5 ternary system. The characteristic signatures of the order (degree of order, domain size, c/a ratio), the density and microstructure, and the dielectric loss properties were monitored for small changes in the bulk composition. These results, collected from over 35 different samples, were used to map the change in $Q \times f$ over a narrow single-phase region that was identified for BZN. Although the structure could only tolerate quite small levels ($<2\%$) of vacancies on the A or B sites, they brought about very large changes in the stability and kinetics of the cation ordering and the resultant $Q \times f$ values. In particular, it was found that the highest $Q \times f$s did not occur at the stoichiometric composition (where $Q \times f \sim 75\,000$) but in single-phase non-stoichiometric samples lying along the $Ba_5Nb_4O_{15}$ and $BaNb_2O_6$ lines. The study also included a partial analysis of the effect of compositional changes on the structure and properties of the BZN–BW solid solutions described previously.[1]

II. Experimental Procedure

Non-stoichiometric BZN solid solutions (listed in Table I) were prepared by standard solid-state synthesis methods using high-purity oxide or carbonate powders, following procedures similar to those used for the study of pure BZN and BZN–BW.[1] The effect of BaO and ZnO non-stoichiometry was also studied for the BZN–BW system ($(1-x)Ba_3ZnNb_2O_9$–$xBa_3W_2O_9$) where the concentration of BW was fixed at $x = 0.01$. All of the BZN solid solutions were sintered into dense ceramics at 1420°C for 4 h, while BZN–BW could be sintered at 1390°C for 4 h. After sintering, the samples were annealed at 1300°C for 24 h (BZN) or 12 h (BZN–BW). The loss of ZnO was avoided by burying the samples in powders of their own composition—see Wu and Davies.[1] for details—and no losses or gains in weight were observed during the processing.

X-ray diffraction (XRD) patterns were collected with a Rigaku diffractometer using a Cu$K\alpha$ source operated at 45 kV and 30 mA. Lattice parameters were calculated by least-squares refinement of powder diffraction data in the range of 10°–150°, collected using silicon powder as an internal standard. The microstructures were examined on the polished and thermally etched ceramics, and fragment samples using a JEOL 6300F FEG HRSEM (JEOL USA Inc., Peabody, MA) operated at 10 kV. Energy dispersive X-ray spectrometer (EDS) (Oxford Instruments Concord Nanoanalysis, Concord, MA) analysis was conducted with a JEOL 6400 Analytical scanning electron microscopy (SEM) equipped with an Oxford EDS and wavelength dispersive X-ray spectrometer (WDS). The dielectric properties were measured by standard cavity methods in the $TE_{01\delta}$ mode using an Agilent HP8720ES network analyzer.

Table I. Compositions (mole ratio) of the investigated non-stoichiometric (a) BZN perovskites and (b) BZN–BW perovskites

	x	BaO	ZnO	Nb_2O_5
(a) BZN perovskites				
BZN	0	0.60	0.20	0.20
BZN–xBaO	0.005	0.6012	0.1994	0.1994
(BaO excessive)	0.01	0.6024	0.1988	0.1988
	0.03	0.6071	0.1965	0.1965
BZN–$xZn_{1/3}Nb_{2/3}O_2$	0.005	0.5988	0.2006	0.2006
(BaO deficient)	0.01	0.5976	0.2012	0.2012
	0.02	0.5952	0.2024	0.2024
	0.005	0.5994	0.2008	0.1998
BZN–xZnO	0.01	0.5988	0.2016	0.1996
(ZnO excessive)	0.02	0.5976	0.2032	0.1992
	0.04	0.5952	0.2064	0.1984
	0.06	0.5929	0.2095	0.1976
BZN–$xBaNb_{2/3}O_{8/3}$	0.03	0.6036	0.1952	0.2012
(ZnO deficient)	0.045	0.6054	0.1927	0.2018
	0.06	0.6073	0.1903	0.2024
BZN–$xNb_{2/3}O_{5/3}$	0.005	0.5994	0.1998	0.2008
(Nb_2O_5 excessive)	0.01	0.5988	0.1996	0.2016
	0.02	0.5976	0.1992	0.2032
BZN–$xBaZn_{1/3}O_{4/3}$	0.005	0.6006	0.2002	0.1992
(Nb_2O_5 deficient)	0.01	0.6012	0.2004	0.1984
	0.02	0.6024	0.2008	0.1968
BZN–$xBa_{4/3}Nb_{2/3}O_3$	0.006	0.6012	0.1988	0.2000
	0.01	0.6020	0.1980	0.2000
	0.03	0.6060	0.1940	0.2000
	0.06	0.6120	0.1880	0.2000
BZN–$xBaNb_{4/5}O_3$	0.02	0.6019	0.1966	0.2015
	0.04	0.6039	0.1932	0.2029
	0.06	0.6058	0.1898	0.2044
BZN–$xBa_{1/2}NbO_3$	0.005	0.5997	0.1994	0.2009
	0.008	0.5996	0.1990	0.2014
	0.01	0.5994	0.1988	0.2018
	0.02	0.5988	0.1976	0.2036
BZN–$xBaZn_{1/2}Nb_{1/2}O_{2.75}$	0.04	0.5988	0.2036	0.1976
	0.08	0.5976	0.2072	0.1952
	0.12	0.5964	0.2107	0.1928
	0.2	0.5941	0.2178	0.1881
	0.4	0.5882	0.2353	0.1765

	x	BaO	ZnO	Nb_2O_5	WO_3
(b) BZN–BW perovskites					
0.99 BZN–0.01 BW	0	0.6	0.198	0.198	0.0040
BaO excess	0.0033	0.6008	0.1976	0.1976	0.0040
	0.01	0.6024	0.1968	0.1968	0.0040
BaO deficient	−0.0033	0.5992	0.1984	0.1984	0.0040
	0.01	0.5976	0.1992	0.1992	0.0040
ZnO excess	0.02	0.5976	0.2012	0.1972	0.0040
	0.04	0.5952	0.2044	0.1964	0.0040
	0.06	0.5929	0.2075	0.1957	0.0040
ZnO deficient	−0.0033	0.6012	0.1964	0.1984	0.0040
	−0.01	0.6036	0.1932	0.1992	0.0040
	−0.015	0.6054	0.1907	0.1998	0.0040
	−0.02	0.6073	0.1883	0.2004	0.0040

III. Results

(1) Phase Stability and Order

The extent of any non-stoichiometry in $Ba(Zn_{1/3}Nb_{2/3})O_3$ was explored along 10 pseudo-binary lines in the BaO–ZnO–Nb_2O_5 ternary system; a summary of the actual compositions and their position in the ternary system is given in Table I and Fig. 1. They include BZN with an excess and deficiency of each of the

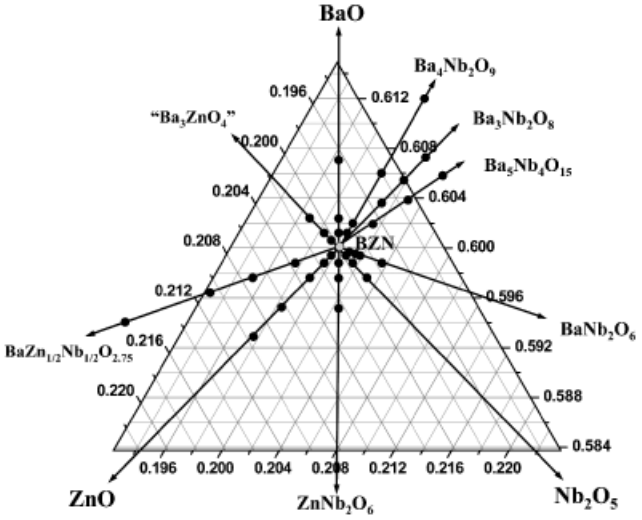

Fig. 1. Directions and compositions investigated in the BaO–ZnO–Nb_2O_5 ternary system.

component end-members (BaO, Nb_2O_5, and ZnO), pseudo-binaries with three barium niobates ($Ba_4Nb_2O_9$, $Ba_5Nb_4O_{15}$, and $BaNb_2O_6$), and the pseudo-binary between BZN and a ternary composition "$Ba_2ZnNbO_{5.5}$". The effect of BaO and ZnO non-stoichiometry was also studied for the BZN–BW; see the compositions given inTable I(b). The XRD patterns of the non-stoichiometric samples cited below were all collected on crushed pellets equilibrated at 1300°C for $\geq$ 24 h (BZN) and 12 h (BZN–BW), respectively.

(A) BaO–BZN: Compositions of BZN with excess BaO lie along the (x)BaO–$(1–x)BaZn_{1/3}Nb_{2/3}O_3$ pseudo-binary; those deficient in BaO actually lie along the pseudo-binary between zinc niobate ($ZnNb_2O_6$) and BZN and were prepared according to the stoichiometry $(x)Zn_{1/3}Nb_{2/3}O_2$–$(1–x)BaZn_{1/3}Nb_{2/3}O_3$. The X-ray patterns of the deficient (negative values of x) and excess (positive x) BaO samples are shown in Fig. 2(a). For x values within the range $-0.01 \leq x \leq +0.01$, the patterns were free of peaks from impurity phases; beyond this range, additional reflections could be assigned to $Ba_4Nb_2O_9$ ($x > +0.01$) and a recently discovered barium zinc niobate tetragonal tungsten bronze ($x < -0.01$) [T.A. Vanderah, NIST, Private communication], respectively. There were large changes in the strength of the 1:2 ordering reflections of BZN within the very narrow single phase forming region. The dependence of the relative intensity of the $(100)_{order}$ reflection on x is shown in Fig. 2(b). Relative to pure BZN, small degrees of BaO deficiency increase the degree of order, while all the excess BaO compositions are completely disordered. Table II lists the lattice parameters of these samples refined from XRD data collected over a range of 2θ from 10° to 150°. The unit cell volumes of the disordered BaO-excess phases show clearly detectable increases in volume that are also apparent from the shift of the peaks in the high-angle regions of the X-ray patterns (Fig. 2(c)).

The effect of BaO non-stoichiometry was also investigated for the BZN–BW perovskite, $Ba[(Zn_{0.99}Vac_{0.01})_{1/3}(Nb_{0.99}W_{0.01})_{2/3}]O_3$. The patterns, Fig. 3, were free of peaks from secondary phases in a narrow range with $-0.0033 \leq x \leq +0.0033$. Consistent with the behavior of pure BZN, a small increase in the intensity of $(100)_{order}$ was measured for negative x and complete disorder was induced by excess BaO (Fig. 3(b)). Similar expansions of the unit cell volume were detected from the cell parameters, Table III, and the high-angle peak shifts (Fig. 3(c)).

(B) ZnO–BZN: Compositions of ZnO-rich BZN (positive x) lie along the (x)ZnO–$(1–x)BaZn_{1/3}Nb_{2/3}O_3$ tie line; those with a ZnO deficiency lie along the hypothetical binary between BZN and $Ba_3Nb_2O_8$, and were formulated as $(x)BaNb_{2/3}O_{8/3}$–$(1–x)BaZn_{1/3}Nb_{2/3}O_3$. The X-ray patterns from the samples, Fig. 4, were free of secondary phases between $-0.02 \leq x \leq +0.02$. Because the contribution of one mole of ZnO to the stoichiometry of Zn in $BaZn_{1/3}Nb_{2/3}O_3$ was three times that of $BaNb_{2/3}O_{8/3}$, the actual range of solid solution in $(x)BaNb_{2/3}O_{8/3}$–$(1–x)BaZn_{1/3}Nb_{2/3}O_3$ was $0 \leq x \leq 0.06$. The changes in the ordering peaks were minimal for the narrow range of ZnO deficiency; on the ZnO-rich side, the ordering peaks systematically weakened and were absent in $x = 0.06$; see Fig. 4(b). The onset of disorder for the ZnO-excess samples was accompanied by a small increase in cell volume, and by a small but systematic movement of the high-angle peaks to lower angles (Fig. 4(c)).

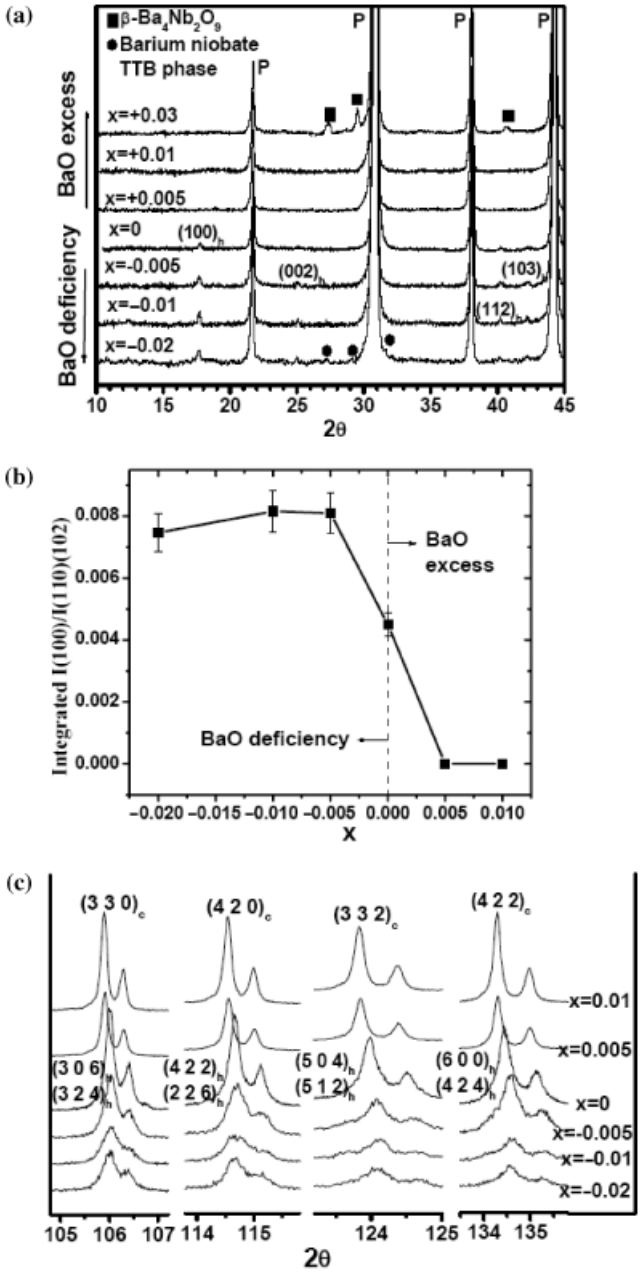

Fig. 2. Diffraction data for BaO-deficient (negative x) and excess (positive x) $Ba(Zn_{1/3}Nb_{2/3})O_3$ (BZN) after annealing at 1300°C for 24 h; (a) X-ray diffraction (XRD) patterns; (b) integrated relative intensity of $(100)_{order}$; (c) high-angle regions of the XRD patterns showing peak shifts in the excess BaO samples.

The sample of $(Ba[(Zn_{0.99}Vac_{0.01})_{1/3}(Nb_{0.99}W_{0.01})_{2/3}]O_3)$ in the BZN–BW system showed similar responses to the introduction of ZnO non-stoichiometry. Within the range $-0.01 \leq x \leq +0.06$, there was no evidence for secondary phases in the X-ray patterns (Fig. 5). The range of ZnO deficiency was slightly narrower than that for pure BZN, presumably because the structure already contained 1% Zn vacancies from the substitution of W^{6+}. The order was maintained on the ZnO-deficient side, and

Table II. Lattice Parameters of Non-Stoichiometric BZN Perovskites

	x	a(Å)	c(Å)	V_{super}(Å^3)	V_{sub}(Å^3)	c/a
Ba site						
	−0.02	5.785	7.0888	205.45	68.482	1.2254
BaO deficient	−0.01	5.7839	7.0884	205.36	68.453	1.2255
	−0.005	5.7847	7.0872	205.39	68.463	1.2252
BZN	0 (order)	5.7854	7.0860	205.40	68.467	1.2248
	0 (disorder)	4.0935	—	—	68.594	—
	0.005	4.0947	—	—	68.652	—
BaO excessive	0.01	4.09495	—	—	68.667	—
	0.03	4.0949	—	—	68.665	—
Zn-site						
	−0.06	5.7852	7.0863	205.39	68.463	1.2249
ZnO deficient	−0.045	5.7855	7.0867	205.42	68.473	1.2249
	−0.01	5.7858	7.0865	205.44	68.480	1.2248
BZN	0(order)	5.7854	7.0860	205.40	68.467	1.2248
	0.02	5.7870	7.0873	205.66	68.553	1.2247
ZnO excessive	0.04	5.7888	7.0890	205.78	68.593	1.2247
	0.06	4.0937	—	—	68.606	—
Nb-site						
	−0.02	4.0948	—	—	68.658	—
Nb_2O_5 deficient	−0.01	4.0946	—	—	68.649	—
	−0.005	4.0945	—	—	68.643	—
BZN	0(disorder)	4.0935	—	—	68.594	—
	0(order)	5.7854	7.0860	205.40	68.467	1.2248
	0.005	5.7813	7.0977	205.48	68.493	1.2277
Nb_2O_5 excessive	0.01	5.7795	7.0991	205.36	68.453	1.2283
	0.02	5.7795	7.0998	205.38	68.460	1.2284

again progressively reduced as the degree of excess ZnO was increased; see Figs. 5(b) and (c).

(C) Nb_2O_5–BZN: Samples with an excess and deficiency of Nb_2O_5 were prepared along the $(x)NbO_{2.5}$–$(1–x)BaZn_{1/3}Nb_{2/3}O_3$ line (positive x) and along a line from BZN toward "Ba_3ZnO_4" (which is not a single-phase compound) where they were formulated as (x)"$BaZn_{1/3}O_{4/3}$"$-(1–x)BaZn_{1/3}Nb_{2/3}O_3$ (negative x). The XRD patterns of the Nb_2O_5-deficient samples were free of impurity peaks up to $x = -0.02$; in the excess Nb_2O_5-direction, the solubility was extremely low and a "clean" sample could only be obtained at $x = +0.005$; see Fig. 6. It should be noted that the concentration of excess Nb cations introduced by the substitution of 1 mole of $NbO_{2.5}$ is equivalent to the concentration of Nb vacancies introduced by 1.5 moles of "$BaZn_{1/3}O_{4/3}$". Therefore, the imbalance in the two directions of non-stoichiometry was even greater than that represented by the x values used above. The secondary phase detected in the Nb-rich compositions could be assigned to a barium zinc niobate tetragonal tungsten bronze formed along the $Ba_3ZnNb_2O_9$–$BaNb_2O_6$ pseudo-binary (T.A. Vanderah, NIST, Private communication).

In contrast to the BaO- and ZnO-deficient solutions, the Nb_2O_5-deficient samples were completely disordered (Figs. 6(a) and (b)). Confirmation of the existence of the narrow region of non-stoichiometry came from a small but systematic change in the lattice parameters for negative values of x; see Table III and Fig. 6(c). Although any non-stoichiometry in the excess Nb_2O_5 direction was clearly extremely narrow, the superlattice reflections showed a very large increase in intensity (Fig. 6(b)). The XRD patterns also showed a large increase in the splitting of the high-angle $(422)_h$ and $(226)_h$ reflections consistent with the formation of a well-ordered structure with a c/a ratio (~ 1.228) that is much larger than well-ordered pure BZN. The c/a ratio was found to continue to increase in the $x = +0.01$ and $+0.02$ samples (Fig. 6(c), Table III) where additional phases were clearly present in the X-ray patterns. This implies that the actual composition of the non-stoichiometric primary perovskite phase in these samples lies in a different part of the small single-phase region of BZN.

(D) $Ba_4Nb_2O_9$–BZN: During the first investigations of the high Q 1:2 ordered tantalate perovskite, $Ba(Zn_{1/3}Ta_{2/3})O_3$, Desu and O'Bryan[9] proposed that the increase in ordering and c/a observed during the later stages of annealing was due to the replacement of the volatilized Zn^{2+} on the B site by the transfer of Ba^{2+} from the A site, which increased the size difference of the ordered "Zn(/Ba)" and Nb sites. This direction of non-stoichiometry corresponds to the formation of a partial solid solution between BZN and $Ba_4Nb_2O_9$ (a non-perovskite phase with three polymorphic modifications). Because $Ba_4Nb_2O_9$ can be rewritten in terms of an ABO_3 perovskite stoichiometry as $BaBa_{1/3}Nb_{2/3}O_3$, the samples were formulated as $(x)BaBa_{1/3}Nb_{2/3}O_3$ $-(1–x)BaZn_{1/3}Nb_{2/3}O_3$. The XRD patterns (Fig. 7(a)) indicated that a small range of single-phase solid solution ($0 < x \leq 0.006$) could be formed in this pseudo-binary system. However, in contradiction to the previous suggestion for BZT, the 1:2 ordering peaks were completely eliminated for even the smallest additions of $Ba_4Nb_2O_9$. No evidence for the development of 1:2 order was found even after annealing at 1300°C for more than 30 h. The formation of a non-stoichiometric disordered solid solution in this direction was accompanied by a relatively large expansion in the lattice parameter of the $x = 0.006$ composition (Table IV(a)), which is evident from shifts in the high-angle reflections (Fig. 7(b)) that are comparable to those observed in BaO-excess BZN.

(E) $Ba_5Nb_4O_{15}$–BZN: The formation of non-stoichiometric cation contents was also studied along the $Ba_5Nb_4O_{15}$—BZN binary. $Ba_5Nb_4O_{15}$ is a vacancy containing hexagonal perovskite and can be rewritten as $Ba(\square_{1/5}Nb_{4/5})O_3$, with compositions in the binary then being represented as $(x)Ba(\square_{1/5}Nb_{4/5})O_3$–$(1–x)Ba(Zn_{1/3}Nb_{2/3})O_3$. In the corresponding tantalate system, a ternary hexagonal perovskite, $Ba_8Zn_1Ta_6O_{24}$, has recently been reported;[17,18] this composition corresponds to $x = 5/8$. The formation of the corresponding compound in the BZN system was not explored in detail. The XRD patterns indicated that non-stoichiometric cubic perovskites could be formed for $0 < x \leq 0.04$ (Fig. 8(a)); for higher x, the patterns contained $Ba_5Nb_4O_{15}$ as the secondary phase. The single-phase compositions exhibited a well-developed 1:2 ordered structure and the

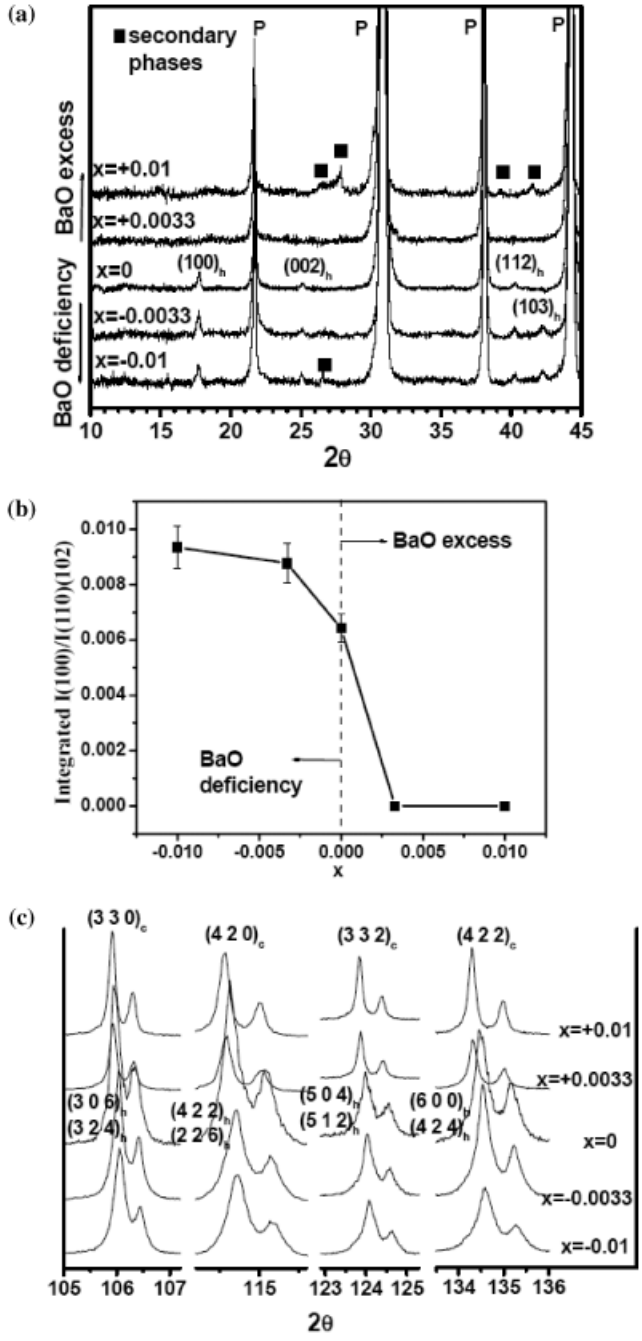

Fig. 3. Diffraction data for BZN–BW with an excess (positive x) and deficiency (negative x) of BaO after annealing at 1300°C for 12 h; (a) X-ray diffraction (XRD) patterns; (b) integrated relative intensity of $(100)_{order}$; (c) high-angle regions of the XRD patterns.

$(100)_{order}$ reflections were much stronger than for pure BZN annealed under the same conditions; see Fig. 8(b). The splitting of the high-angle $(226)_h$ and $(422)_h$ reflections increased systematically with x, and the lattice parameter refinements, Table IV, confirmed that the c/a distortion reached values close to 1.229, the highest reported for this system.

(F) $BaNb_2O_6$–BZN: $BaNb_2O_6$ is another commonly encountered Zn-deficient impurity phase (with a tetragonal tungsten bronze (TTB) structure) along the $BaO–Nb_2O_5$ binary. Compositions along the BZN—$BaNb_2O_6$ join can be formulated as $(x)Ba_{1/2}NbO_3$–$(1–x)BaZn_{1/3}Nb_{2/3}O_3$. The other TTB phase recently found in the ternary system forms at $x = 0.19$–0.20. The range over which impurity-free cubic perovskite patterns were obtained was quite limited and extended no further than $x = 0.008$ (see Fig. 9). Even though the range of stability

Table III. Lattice Parameters of Non-Stoichiometric BZN–BW perovskites

	x	a(Å)	c(Å)	V_{super}(Å^3)	V_{sub}(Å^3)	c/a
A site						
BaO deficient	−0.01	5.7838	7.0870	205.31	68.44	1.22532
	−0.0033	5.7824	7.0874	205.23	68.41	1.22569
BZN–BW	0(order)	5.7836	7.0869	205.29	68.43	1.22534
BaO excessive	0.0033	4.0942	—	—	68.63	—
	0.01	4.0951	—	—	68.67	—
B-site						
	−0.015	5.7843	7.0872	205.35	68.45	1.22525
ZnO deficient	−0.01	5.7839	7.0874	205.33	68.44	1.22537
	−0.0033	5.7838	7.0873	205.32	68.44	1.22536
BZN–BW	0	5.7836	7.0869	205.29	68.43	1.22534
	0.02	5.7855	7.0886	205.48	68.49	1.22524
ZnO excessive	0.04	5.7888	7.0889	205.73	68.58	1.22459
	0.06	5.7894	7.0882	205.74	68.58	1.22434

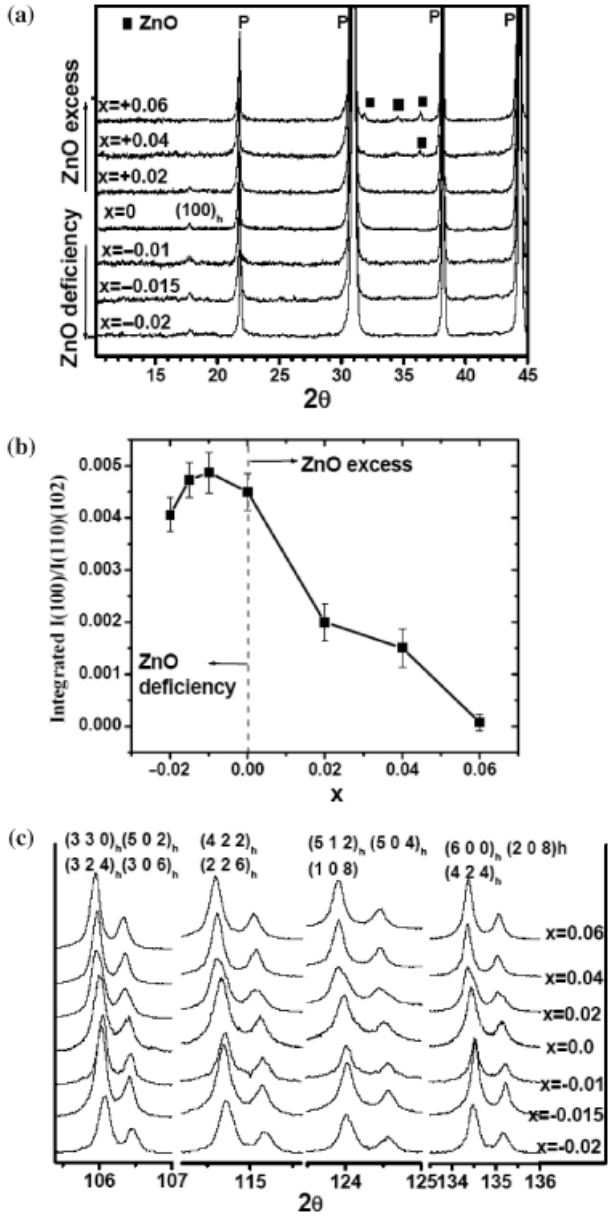

Fig. 4. Diffraction data for $Ba(Zn_{1/3}Nb_{2/3})O_3$ (BZN) with an excess (positive x) and deficiency (negative x) of ZnO after annealing at 1300°C for 24 h; (a) X-ray diffraction (XRD) patterns; (b) integrated relative intensity of $(100)_{order}$; (c) high-angle regions of the XRD patterns.

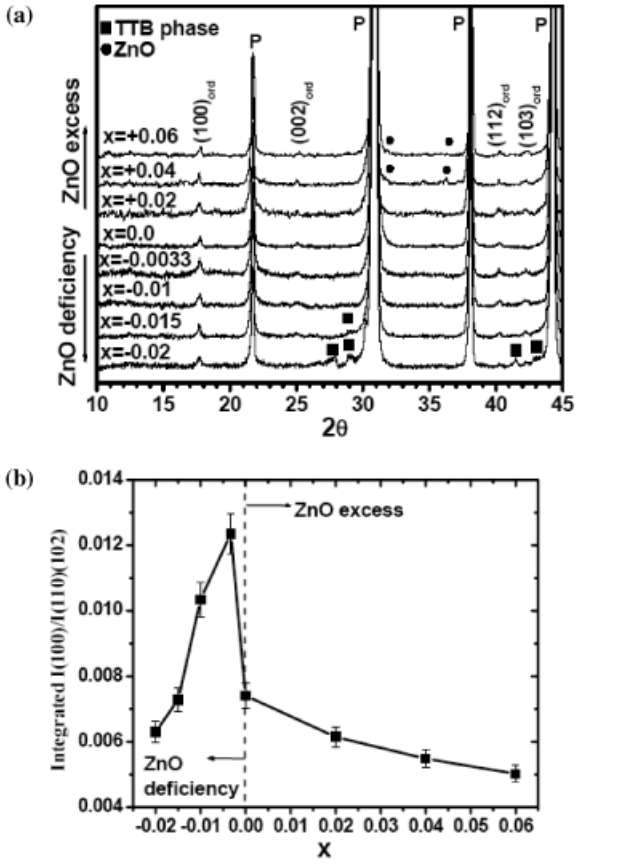

Fig. 5. Diffraction data for BZN–BW with an excess (positive x) and deficiency (negative x) of ZnO after annealing at 1300°C for 12 h; (a) X-ray diffraction (XRD) patterns; (b) integrated relative intensity of $(100)_{order}$; (c) high-angle regions of the XRD patterns.

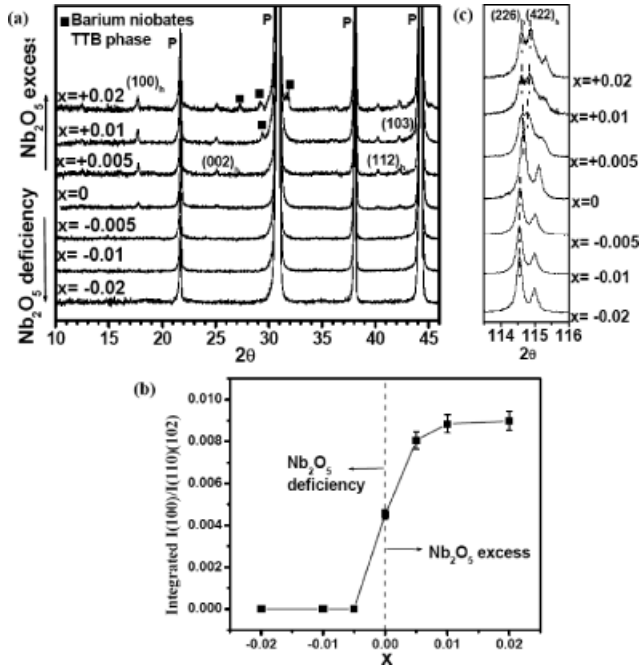

Fig. 6. Diffraction data for $Ba(Zn_{1/3}Nb_{2/3})O_3$ (BZN) with an excess (positive x) and deficiency (negative x) of Nb_2O_5 after annealing at 1300°C for 24 h; (a) X-ray diffraction (XRD) patterns; (b) integrated relative intensity of $(100)_{order}$; (c) high-angle regions of the XRD patterns.

was very narrow, large changes were again observed in the strength of the ordering reflections, which increased significantly for very small x values (0.005)—see Fig. 9(b). The splitting of the $(226)_h$ and $(422)_h$ peaks also increased, and the cell parameters again provided evidence for a large increase in c/a (Table IV, Fig. 9(c)).

(G) "$Ba_2ZnNbO_{5.5}$"–BZN: Although the ternary compound, $Ba_2(ZnNb)O_{5.5}$, is not a stable phase in the BZN ternary system, its tantalate analog forms a stable perovskite where, at a low temperature, Zn and Ta adopt an ordered double perovskite arrangement.[19] $Ba_2(ZnNb)O_{5.5}$ lies within the $(1–x)BaZn_{1/3}Nb_{2/3}O_3–xBaZnO_2$ binary at $x = 0.25$. Although single-phase $Ba_2(ZnNb)O_{5.5}$ could not be prepared either by prolonged heating at a low temperature or by quenching from a high temperature, relatively extended solid solutions could be formed with BZN. Samples along this line were prepared with the general stoic-

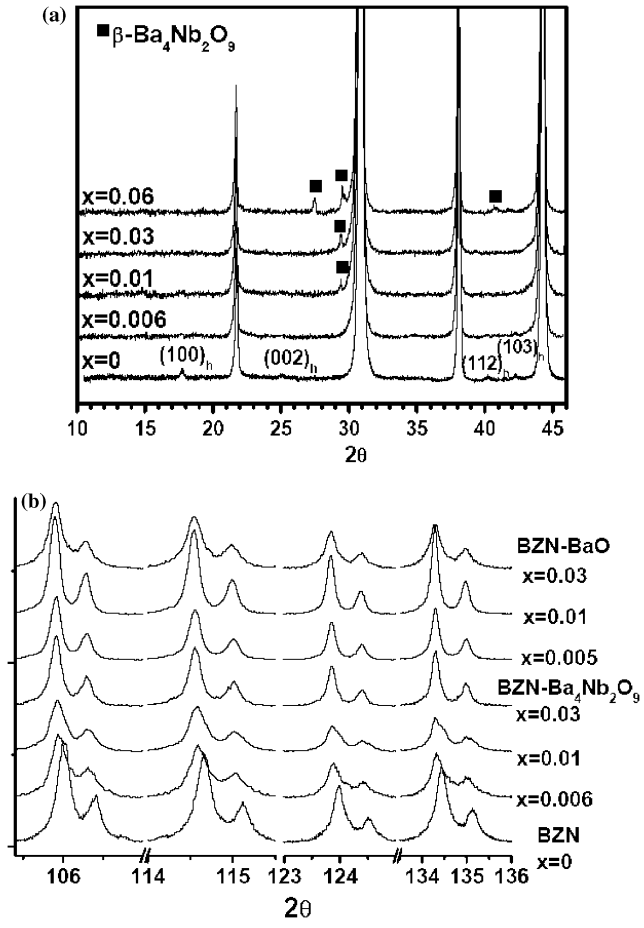

Fig. 7. Low-angle (a) and high-angle (b) region X-ray patterns for $(1–x)Ba_3ZnNb_2O_9–(x)Ba_4Nb_2O_9$ (i.e., $Ba(Zn_{1/3}Nb_{2/3})O_3–Ba_{4/3}Nb_{2/3}O_3$).

Table IV. Lattice parameters of (a) $(1-x)$ $BaZn_{1/3}Nb_{2/3}O_3$–$xBaBa_{1/3}Nb_{2/3}O_3$, (b) $(1-x)$ $BaZn_{1/3}Nb_{2/3}O_3$–$xBa_{1/5}Nb_{4/5}O_3$, (c) $(1-x)$ $BaZn_{1/3}Nb_{2/3}O_3$–$xBa_{1/2}NbO_3$ and (d) $(1-x)$ $BaZn_{1/3}Nb_{2/3}O_3$–$xBaZn_{1/2}Nb_{1/2}O_{2.75}$

	x	a(Å)	c(Å)	V_{super}(Å^3)	V_{sub}(Å^3)	c/a
(a) (1−x) $BaZn_{1/3}Nb_{2/3}O_3$–$xBaBa_{1/3}Nb_{2/3}O_3$						
$Ba[Zn_{1/3}Nb_{2/3}]O_3$	0 (order)	5.7854	7.0860	205.40	68.467	1.2248
	0 (disorder)	4.0935			68.594	—
$Ba_3ZnNb_2O_9$–$Ba_4Nb_2O_9$	0.006	4.0940			68.618	—
	0.01	4.0941			68.622	—
	0.03	—			—	—
	0.06	—			—	—
$Ba[Ba_{1/3}Nb_{2/3}]O_3$	1.0	—			—	—
(b) (1−x) $BaZn_{1/3}Nb_{2/3}O_3$–$xBa_{1/5}Nb_{4/5}O_3$						
$Ba[Zn_{1/3}Nb_{2/3}]O_3$	0 (order)	5.7854	7.0860	205.40	68.467	1.2248
	0.02	5.7824	7.0957	205.46	68.487	1.2271
	0.04	5.7803	7.0981	205.38	68.460	1.2280
	0.06	5.7789	7.0997	205.33	68.443	1.2286
(c) (1−x) $BaZn_{1/3}Nb_{2/3}O_3$–$xBa_{1/2}NbO_3$						
$Ba[Zn_{1/3}Nb_{2/3}]O_3$	0 (order)	5.7854	7.086	205.40	68.467	1.2248
	0.005	5.7812	7.0966	205.41	68.470	1.2275
	0.008	5.7802	7.0987	205.40	68.467	1.2281
	0.01	5.7788	7.0995	205.32	68.440	1.2285
	0.02	5.7781	7.0993	205.27	68.423	1.2286
(d) (1−x) $BaZn_{1/3}Nb_{2/3}O_3$–$xBaZn_{1/2}Nb_{1/2}O_{2.75}$						
$Ba[Zn_{1/3}Nb_{2/3}]O_3$	0 (order)	5.7854	7.086	205.40	68.467	1.2248
	0 (disorder)	4.0935	—	—	68.594	—
$BaZn_{1/3}Nb_{2/3}O_3$–$BaZn_{1/2}Nb_{1/2}O_{2.75}$	0.04	4.0937	—	—	68.604	—
	0.08	4.0939	—	—	68.613	—
	0.12	4.0941	—	—	68.621	—
$Ba[Zn_{1/2}Nb_{1/2}]O_{2.75}$	—	—	—	—	—	—

hiometry $(1-x)Ba(Zn_{1/3}Nb_{2/3})O_3$–$xBa(Zn_{1/2}Nb_{1/2})O_{2.75}$; single-phase perovskites were obtained for $0 \le x \le 0.12$ (Fig. 10). The substitution completely eliminated the 1:2 order (Fig. 10); this is in sharp contrast to ZnO-excess BZN, which is close in composition but sustained the order for small levels of substitution. The lattice parameters of the disordered solid solutions showed a small increase consistent with the increase in the average size of the cations on the B-site; see Table IV.

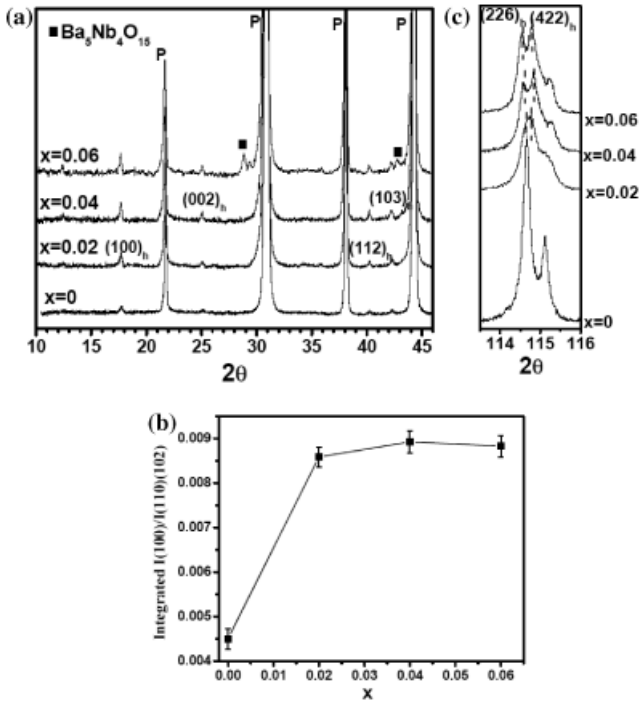

Fig. 8. (a) X-ray diffraction (XRD) patterns of $(1-x)Ba(Zn_{1/3}Nb_{2/3})O_3$–$(x)BaNb_{4/5}O_3$; (b) integrated relative intensity of $(100)_{order}$; (c) splitting of the $(226)_h$ and $(422)_h$ reflections. Samples were equilibrated at 1300°C for 24 h.

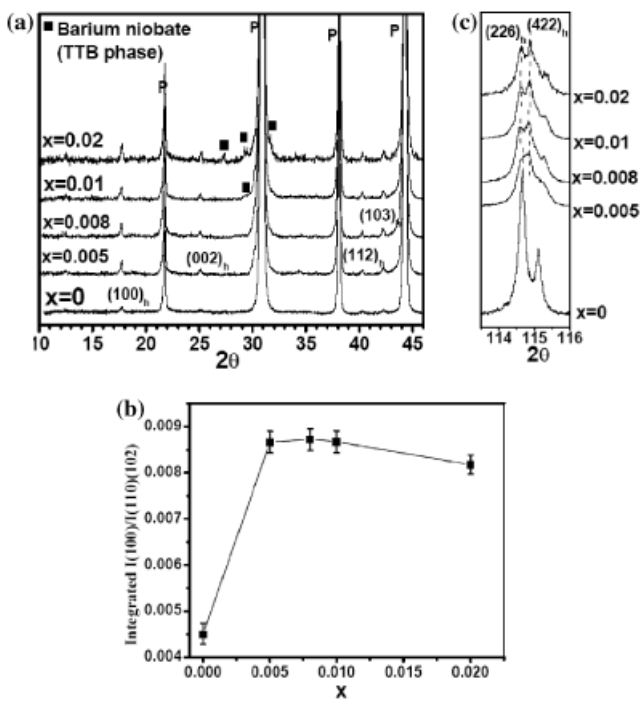

Fig. 9. (a) X-ray diffraction (XRD) patterns of $(1-x)Ba(Zn_{1/3}Nb_{2/3})O_3$–$(x)Ba_{1/2}NbO_3$; (b) integrated relative intensity of $(100)_{order}$; (c) splitting of the $(226)_h$ and $(422)_h$ reflections. Samples were equilibrated at 1300°C for 24 h.

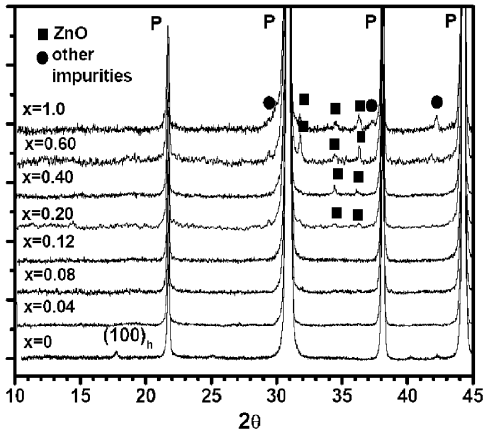

Fig. 10. X-ray diffraction (XRD) patterns of $(1-x)Ba(Zn_{1/3}Nb_{2/3})O_3$ $(x)Ba(Zn_{1/2}Nb_{1/2})O_{2.75}$ after equilibration at 1300°C for 24 h; the pattern of $Ba(Zn_{1/2}Nb_{1/2})O_{2.75}$ ($x = 1.0$) was collected after annealing at 1150°C for 18 h.

In the previous paper on BZN–BW, the c/a distortion of the 1:2 ordered structure was found to be an effective metric of the development of long-range order.[1] Data for the c/a ratios of all the non-stoichiometric BZN solid solutions are summarized in Fig. 11. In the disordered solid solutions, c/a maintains its ideal value of $\sqrt{3}/2$; the highest values were observed for the BZN–$Ba_5Nb_4O_{15}$, BZN–$BaNb_2O_6$, and BZN–Nb_2O_5 joins.

(2) Sintering and Microstructure

The effect of the cation non-stoichiometry on the microstructure was investigated by SEM using ceramics of BZN and BZN–BW sintered for 5 h at 1420° and 1390°C, respectively. A summary of the relative densities of the sintered nonstoichiometric BZN samples is given in Fig. 12. In all cases, appropriate precautions were taken to avoid volatilization of any of the components. Compared with pure BZN,[1] the ceramics with a small amount of BaO deficiency ($x = 0.005$ in $(1-x)$BZN–$(x)Zn_{1/3}Nb_{2/3}O_2$) showed well-developed microstructures with a large grain size ($\sim$10 μm); see Fig. 13(a). However, ceramics with a higher degree of BaO deficiency ($x \geq 0.01$) contained large cavities due to pore coalescence during the very rapid grain growth; see Fig. 13(b). The relative density of these samples was only $\sim$84% (Fig. 12), and not surprisingly they had very low Q's. The grain growth, which arose from the very rapid diffusion of the A-site cations, also severely degraded the microstructures of the BaO-deficient BZN–BW samples. For example, a BZN–BW ceramic with $x = -0.0033$ contained overgrown grains (>10–20 μm); Fig. 14(a); in addition to the exaggerated grain growth, the

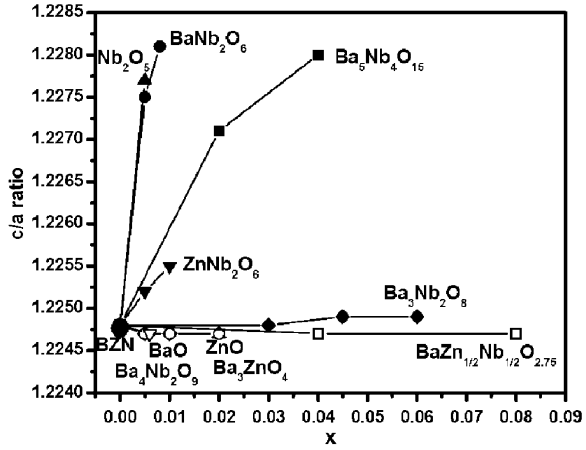

Fig. 11. Lattice distortion (c/a) of all the non-stoichiometric $Ba(Zn_{1/3}Nb_{2/3})O_3$ (BZN) samples after annealing at 1300°C for 24 h.

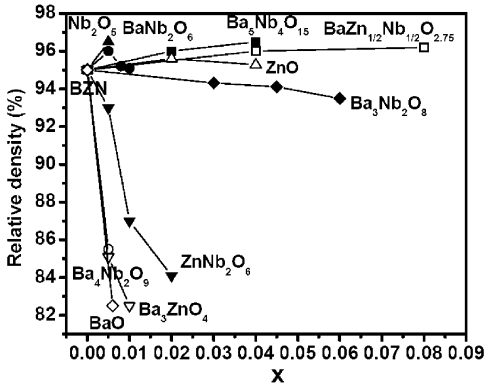

Fig. 12. Relative densities of the sintered (1420°C for 5 h) non-stoichiometric $Ba(Zn_{1/3}Nb_{2/3})O_3$ (BZN) ceramics.

grain boundaries in this sample became highly faceted, and "ghost line" boundaries, which revealed the initial locations of the migrated grain boundaries, were apparent within the grains, Fig. 14(a). These features are signatures of "diffusion induced (or chemically induced) grain boundary migration" (DIGM), which is commonly observed when the sintering involves a liquid phase and one of the species exhibits very rapid diffusion.[20,21]

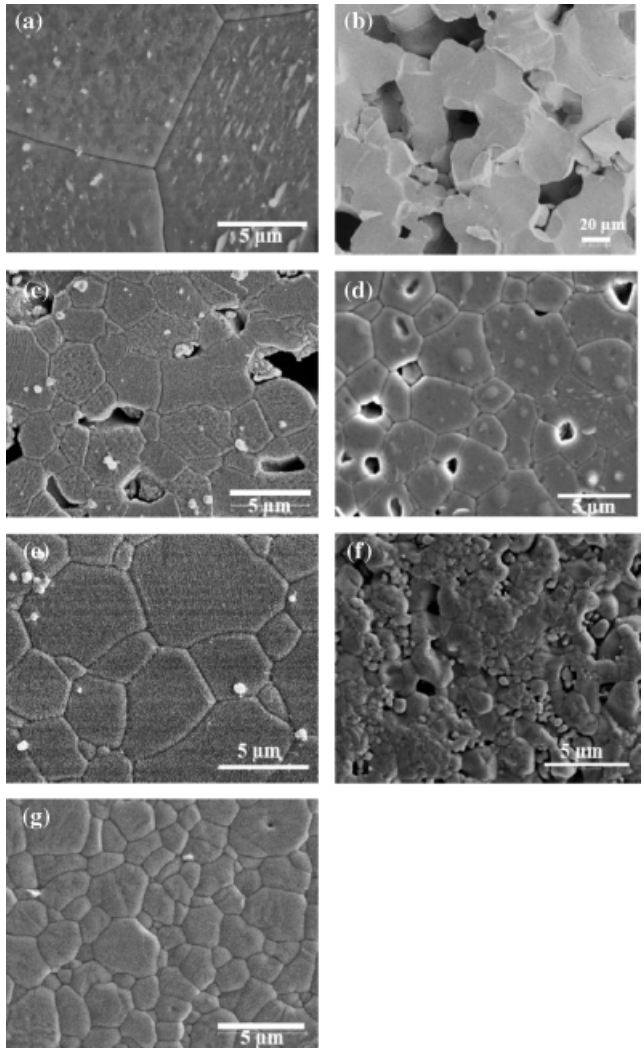

Fig. 13. SEM images of $Ba(Zn_{1/3}Nb_{2/3})O_3$ (BZN) after sintering at 1420°C for 5 h: (a) BaO deficient, $x = -0.005$; (b) BaO deficient, $x = -0.01$; (c) BaO excess, $x = 0.005$; (d) ZnO deficient, $x = -0.015$; (e) ZnO excess, $x = 0.02$; (f) Nb_2O_5 deficient, $x = -0.005$; (g) Nb_2O_5 excess, $x = 0.005$.

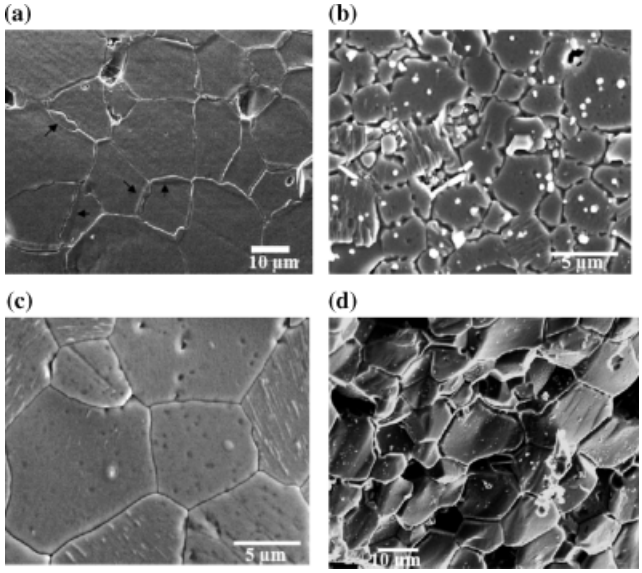

Fig. 14. SEM images of BZN–BW after sintering at 1390°C for 5 h: (a) BaO deficient, $x = -0.0033$; (b) BaO excess, $x = 0.0033$; (c) ZnO deficient, $x = -0.015$; (d) ZnO excess, $x = 0.02$.

The addition of excess BaO to BZN and BZN–BW also inhibits sintering and reduces the density to ~82%. In both systems, the grain sizes were <5 μm; Figs. 13(c) and 14(b). The limited diffusion in the excess BaO systems is consistent with previous studies of BZT [22] and BMT,[2] where small levels of segregation of the Ba solute ion to the grain boundaries were found to decrease the grain growth through a "solute drag" effect.

In contrast to the observations in BMT[2] and BMN,[4] but consistent with the studies of BZT,[10] a ZnO deficiency does not significantly change the grain growth or bulk density of BZN or BZN–BW. The grain sizes are similar to stoichiometric BZN (~1–3 μm) and BZN–BW (~5–8 μm). Although the sintering of stoichiometric BZN–BW proceeds via a liquid-phase sintering mechanism, the ZnO-deficient BZN–BW showed no evidence for the involvement of a liquid phase and the small change in stoichiometry apparently shifts the temperature of the peritectic reaction identified in our first paper.

Compositions of BZN with excess ZnO are well densified (~95%), in agreement with previous data for BZT.[10] The SEM image (Fig. 13(e)) reveals a structure with a larger grain size (~3–6 μm) compared with the other BZN compositions. EDS analysis showed that some grain boundary regions were rich in Zn; this is consistent with the XRD data for these samples (Fig. 3) where ZnO was detected as a secondary phase. For the ZnO-excess BZN–BW ceramics, a liquid phase was clearly visible in the grain boundary and the average grain size increased to 10 μm; see Fig. 14(d).

The microstructures of the Nb_2O_5-deficient ceramics (Fig. 13(f)) were similar to those with excess BaO, and limited grain growth led to poor densities (<86%). However, compositions with excess Nb_2O_5 yielded high-density ceramics (96%) with uniform grains in the range ~1–3 μm; see Fig. 13(g).

(3) Dielectric Properties

The dielectric loss properties are extremely sensitive to the changes in B-site order and bulk density. The $Q \times f$ product of BZN with an excess and deficiency of ZnO, BaO, and Nb_2O_5 is shown in Fig. 15 for samples after sintering and after additional annealing. The introduction of a deficiency of ZnO, Fig. 15(a), did not significantly affect $Q \times f$, consistent with the similarity of the degree of order and microstructure to stoichiometric BZN. Even though they exhibited improved densities and large grain sizes, for the excess ZnO ceramics $Q \times f$ was significantly degraded due to the large decrease in the degree of order. The

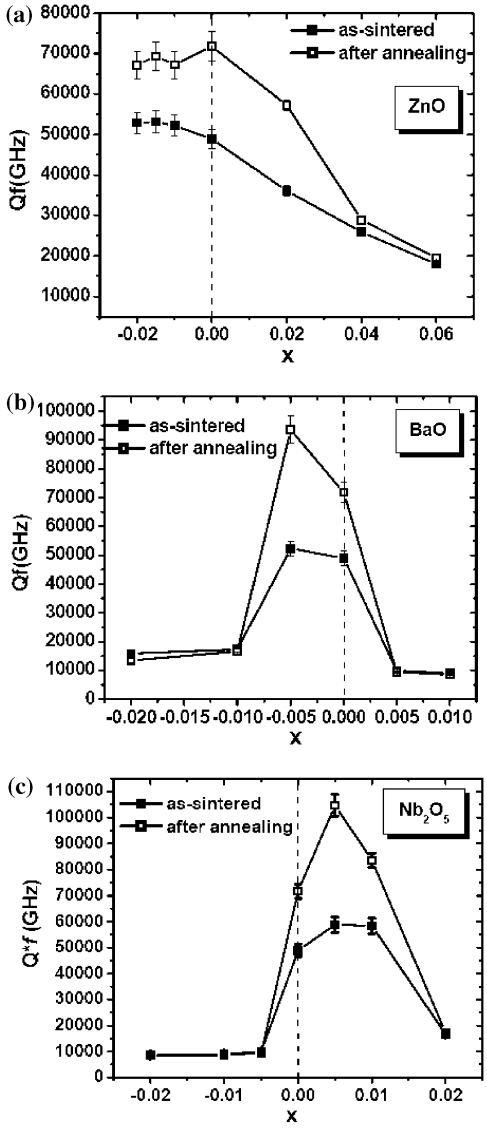

Fig. 15. $Q \times f$ values of $Ba(Zn_{1/3}Nb_{2/3})O_3$ (BZN) with an excess and deficiency of: (a) ZnO; (b) BaO; and (c) Nb_2O_5. As-sintered samples are indicated by solid squares, and annealed samples by open squares.

BaO-deficient samples, which lie along the line with $ZnNb_2O_6$, have a more complicated variation in Q. For small deficiencies ($x = -0.005$), $Q \times f$ increased to ~90 000; this sample also showed an increase in the degree of order. At higher levels of BaO deficiency $Q \times f$ decreased abruptly to ~15 000; it was in this range that the microstructures developed excessive porosity (see Fig. 13(b)). The excess-BaO samples, which are disordered (Fig. 2) and poorly sintered (Fig. 13), had very low $Q \times f$'s for all compositions.

Nb_2O_5-excess ceramics with $x = 0.005$ gave an excellent dielectric response with a $Q \times f \sim 108\,000$ at 8 GHz; this sample had well-developed order and a highly dense microstructure. The reduction in $Q \times f$ for $x \geq 0.01$ coincided with the formation of secondary phases. The disordered and low density Nb_2O_5-deficient ceramics along the Ba_3ZnO_4 line had some of the lowest Q's observed in the system (Fig. 15).

The $Q \times f$ data for BaO- and ZnO-substituted BZN–BW are shown in Fig. 16; the trends are similar to BZN. Well-ordered ZnO-deficient samples with $-0.01 \leq x < 0$ all showed excellent $Q \times f$'s (~105 000) that were slightly higher than pure BZN–BW ($Q \times f = \sim 100\,000$); the deterioration for a larger deficiency ($x \leq -0.015$) coincided with the formation of secondary phases. The $Q \times f$ of ZnO-excess BZN–BW was similar to BZN and decreased rapidly as the cation order was reduced. As expected,

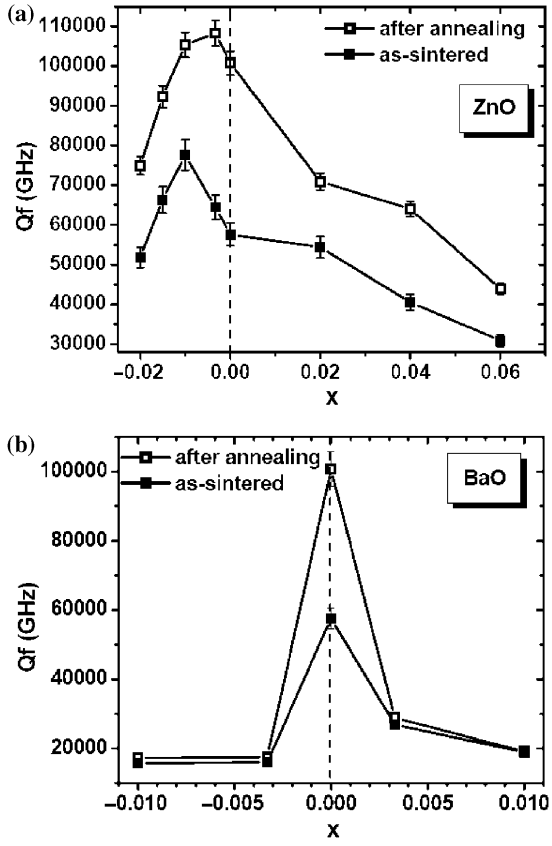

Fig. 16. $Q \times f$ values of BZN–BW with an excess and deficiency of: (a) ZnO and (b) BaO. As-sintered samples are indicated by solid squares, and annealed samples by open squares.

given the extensive DIGM in the microstructure, BaO-deficient BZN–BW had a very low Q ($Q \times f \sim 17\,000$), which did not improve even after prolonged annealing (24 h) at 1300°C. $Q \times f$ also decreased in BaO-excess BZN–BW, which also showed a reduced order and a degraded microstructure.

The $Q \times f$'s measured for the other directions of non-stoichiometry examined for BZN are shown in Fig. 17, which also includes a summary of the BaO, ZnO, and Nb_2O_5 data. The losses almost exactly parallel the trends in cation order and in particular the c/a data in Fig. 11. The largest improvements in Q occured in non-stoichiometric compositions along the $BaNb_2O_6$ and $Ba_5Nb_4O_{15}$ directions, and, as noted above, for small amounts of excess niobia. In all the other pseudo-binary directions, $Ba_3Nb_2O_8$ (which corresponds to ZnO deficiency), $Ba_4Nb_2O_9$, and $BaZn_{1/2}Nb_{1/2}O_{2.75}$ $Q \times f$ was reduced to very low values; in each case, the decrease coincided with the loss of cation order.

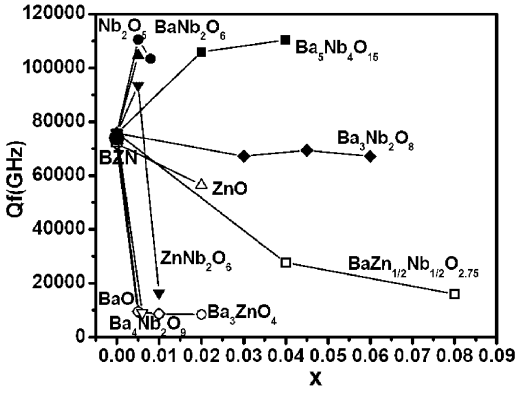

Fig. 17. Summary of $Q \times f$ values of all the investigated single-phase non-stoichiometric samples of BZN after annealing at 1300°C for 24 h.

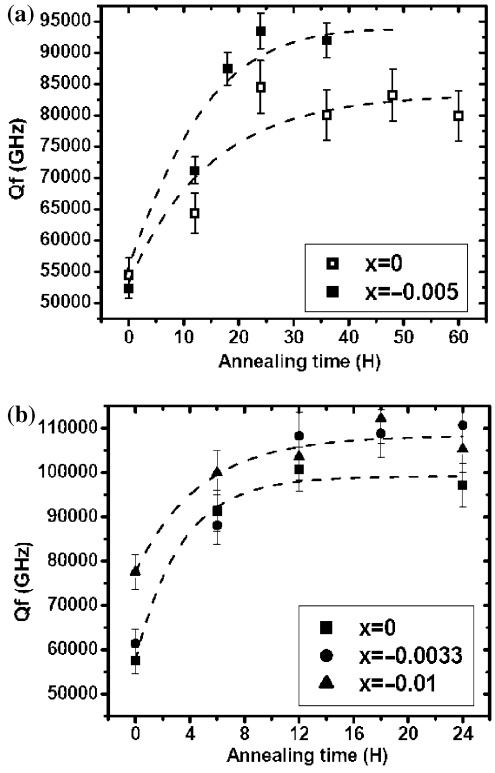

Fig. 18. Variation of $Q \times f$ with the time of annealing at 1300°C for: (a) BaO-deficient $Ba(Zn_{1/3}Nb_{2/3})O_3$ (BZN) ($x = -0.005$) and (b) ZnO deficient BZN—BW ($x = -0.0033$ and $x = -0.01$).

The correlation between the changes in structure and Q is further highlighted by the data in Fig. 18, where the dielectric properties of BaO-deficient BZN ($x = -0.005$) and ZnO-deficient BZN–BW and their pure BZN and BZN–BW counterparts were monitored as a function of the time of annealing at 1300°C. In each case, Q increased systematically with the annealing time and mirrorred the increase in the intensity of the ordering shown in Figs. 2 and 5. Given the similar densities of the ceramics, it is clear that cation ordering rather than grain size is primarily responsible for the improvement in Q.

Although the limited ranges of non-stoichiometry are clearly critical in mediating the dielectric losses, the small changes in chemistry would not be expected to alter significantly the relative dielectric constant or the temperature coefficient of resonant frequency (τ_f) of BZN or of BZN–BW. The experimental values support this conclusion, and the relative dielectric constants lie

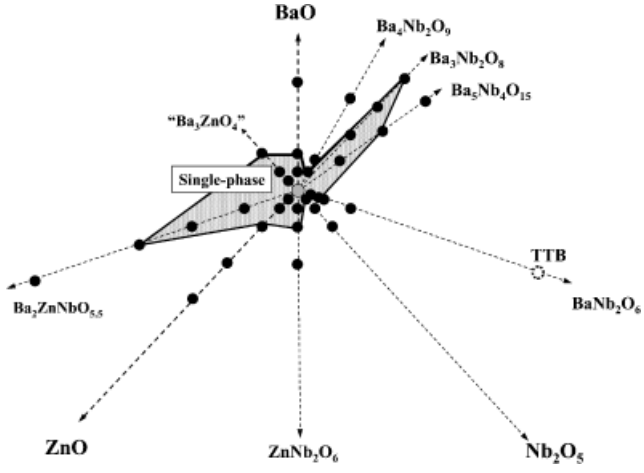

Fig. 19. Observed single-phase cubic perovskite-forming region in the BaO–ZnO–Nb_2O_5 ternary system.

in a narrow range between 37 and 41, and τ_f between $\sim +21$ and 27 ppm/°C. In agreement with many other studies of microwave complex perovskites, for a similar bulk density, the values of ε and τ_f of the ordered phases were slightly lower than their disordered counterparts.

IV. Discussion

The results for the phase stability of BZN (and BZN–BW) show that the perovskite structure can support limited ranges of non-stoichiometry in several directions in the BaO–ZnO–Nb_2O_5 ternary; these are summarized in Fig. 19. Although the non-stoichiometry was very limited, typically 1% or less, in almost cases it was accompanied by small but detectable changes in the cell parameters, and had a very large effect on the extent and stability of the B-site order, the sintering and microstructure, and the microwave dielectric loss properties. The results of the 10 pseudo-binaries that were studied can be used to tailor the bulk composition to produce well-developed 1:2 order, good sintering properties and high density, and a very high Q value for real applications. However, it is clear that these optimized ceramics should not have a stoichiometric bulk chemistry with Ba:Zn:Nb = 3:1:2. In this section, we discuss the effect of the different types of non-stoichiometry on the crystal chemistry and microstructure, and analyze how the two combine to affect the final Q value.

In ZnO-deficient BZN with compositions of $Ba_3Nb_2O_8$, the cation order is maintained within the narrow region of non-stoichiometry. In this range, the Zn and oxygen vacancy containing a 1:2 ordered structure can be represented by $Ba[(Zn_{1-x}\square_{Znx})_{1/3}Nb_{2/3}]O_{3-x/3}\square_{Ox/3}$. In our investigation of the BZN–BW system,[1] the formation of Zn vacancies brought about a large improvement in the order, and very small concentrations increased the temperature of the order–disorder transition of BZN by 35°C. The increase in T_{order} and larger destabilization of the disordered structure were ascribed to the Zn–O–Zn linkages, which were not present in the ordered structure. For these linkages, the formation of a Zn vacancy exacerbated the highly underbonded character of the oxygen anion. Although this argument would imply that ZnO-deficient compositions of BZN should also exhibit increased ordering and a higher T_{order}, this was not observed. Instead, the XRD data showed that the degree of order and c/a, were similar to pure BZN; furthermore, a series of quenching experiments showed that T_{order} for these compositions was $\sim$1375°C, the same as stoichiometric BZN. The primary difference between ZnO–BZN and BZN–BW was the absence of oxygen vacancies in the latter, where the Zn vacancy was charge compensated by the W^{6+} cations. Therefore, the introduction of oxygen vacancies, especially in the Zn–O–Zn linkage, must reduce the destabilization of the disordered structure and the combined effect of Zn and oxygen vacancies does not alter the relative energetics of the two phases or the degree of order.

Zn vacancies are also introduced in the solid solutions along the BZN–$Ba_5Nb_4O_{15}$ binary; however, in this case the oxygen stoichiometry was maintained by the addition of a small excess of Nb^{5+}. The samples in this system showed a large increase in the degree of order, and the structure had one of the highest c/a distortions and highest Q's of all the compositions explored (Figs. 11 and 17). The stoichiometry of these solid solutions is given by $Ba(Zn_{(1-x)}\square_{Znx})_{1/3}Nb_{2(1+x/5)/3}O_3$. In their 1:2 ordered form, the most likely cation distribution would retain full occupancy of the Nb site, with the Zn site accommodating the vacancies and the excess niobium, i.e., $Ba[(Zn_{1-x}\square_{3x/5}Nb_{2x/5})_{1/3}Nb_{2/3}]O_3$. The increase in the relative stability of the order in these phases was confirmed by quenching experiments conducted on a sample with $x = 0.04$ that showed $T_{order} = 1415$°C. This increase is similar in magnitude to the BZN–BW system, and we propose that it is also associated with the large destabilization of the disordered phase by the Zn vacancies, which are no longer compensated by oxygen vacancies.

While formation of B-site vacancies in a cubic perovskite is always limited to a very small range of stability, extensive A-site non-stoichiometry is observed in several compounds (e.g., $La_{2/3}TiO_3$ ($x = 0.33$),[23] $Th_{1/4}NbO_3$.[24–26] However, these examples are confined to simple perovskites with a single highly charged B-site cation, and there are no examples of extensive A-site vacancy formation in complex perovskites where at least one B cation has a low charge. For $Ba(Zn_{1/3}Nb_{2/3})O_3$, only a very limited range ($\sim$1%) of BaO-deficient solutions, along the BZN–$ZnNb_2O_6$ line, could be formed; within this range, the non-stoichiometry was accompanied by an increase in the degree of order (Fig. 2). The Ba vacancies are charge balanced by an equal concentration of oxygen vacancies, and the composition is given by $(Ba_{(1-x)}\square_{Bax})Zn_{1/3}Nb_{2/3}O_{3-x}\square_{Ox}$. The Ba and O vacancies should reduce the overall energetic stability of both the ordered and disordered structures and the underbonded anions in Zn–O–Zn linkages will again be the ones most susceptible to extensive destabilization. For the ZnO-deficient BZN system, the association of Zn and O vacancies apparently mediate the impact of B-site vacancies on the Zn–O–Zn linkages; however, because each zinc is coordinated by six anions there is still a significant probability that Zn–O–$\square_{Zn}$ clusters will still be present in the disordered structure. Because the A sites are coordinated by 12 anions, the formation of a barium vacancy will affect all twelve Ba–O–Ba linkages in the unit cell. Therefore, even if the compensating anion vacancy is in the same unit cell, there is a 100% higher statistical probability that Zn–O–Zn linkages will remain intact and may be affected by the missing Ba cations. Although the impact of the Ba vacancy on the bond valence of oxygen is less than a Zn vacancy (2/12 vs 2/6), it is still likely to be large enough to increase the difference in the free energy of the disordered and ordered structures, as the latter do not contain any Zn–O–Zn linkages. Direct support for this argument comes from quenching experiments of a BaO-deficient sample with $x = 0.01$, which had an order–disorder transition at 1400°C, 10°C lower than the sample with 1% Zn vacancies, but still 25°C higher than pure BZN.

The Ba (and O) vacancies also provide additional pathways for the inter-diffusion of the B-site cations and would be expected to enhance the kinetics of the ordering process and the ordered domain growth. This conclusion is supported by the observation of well-ordered, high c/a structures after a short annealing time and an associated increase in the rate of enhancement in the Q values of these samples during their annealing at 1300°C (Fig. 18).

From the XRD patterns (Figs. 2–5), small amounts of excess-BaO and ZnO weaken or completely eliminate the 1:2 ordering. In previous studies of nonstoichiometric BZT-type perovskites, e.g., $Ba(Mg_{1/3}Ta_{2/3})O_3$,[2] the stoichiometries of BaO or MgO excess BMT were represented as "$Ba_{1+\delta}[Mg_{1/3}Ta_{2/3}]O_{3+\delta}$" and "$Ba[(Mg_{1+\delta})_{1/3}(Ta)_{2/3}]O_{3+\delta/3}$", respectively. While these formulae do represent the composition, they cannot reflect the stoichiometry of the perovskite structure. To maintain ABO_3-type stoichiometry, ZnO-excess BZN can be represented as $(Ba_{(1-x)}\square_{Bax})[Zn_{(1+2x)/3}Nb_{(2-2x)/3}]O_{3-2x}\square_{O2x}$. This formalism is equivalent to describing ZnO as $\square_{Ba}ZnO\square_{O2}$ in an ABO_3 format and representing the direction of solid solution formation as $(1-x)BaZn_{1/3}Nb_{2/3}O_3$-$(x)\square_{Ba}ZnO\square_{O2}$. The addition of excess ZnO introduces Ba and O vacancies into the structure and increases the Zn:Nb stoichiometry to values >1:2. From the above discussion, the Ba vacancies would be expected to promote ordering; however, in the ordered phase the additional Zn cations must occupy the Nb sites to form a structure with $(Ba_{(1-x)}\square_{Bax})[Zn_{1/3}(Zn_xNb_{1-x})_{2/3}]O_{3-2x}\square_{O2x}$. The partial occupancy of the Nb sites by Zn ("Zn_{Nb}") decreases the charge difference (Δq) of the two ordered B sites. 1:2 ordered perovskites have been shown to form only when $\Delta q \geq 3$ [27,28] and substitutions that reduce Δq below 3.0 (e.g., $La(Zn_{2/3}Nb_{1/3})O_3$, which also introduces Zn onto the Nb site [29]) destabilize the order. Apparently, these two factors combine to sustain weak ordering for small amounts of excess ZnO ($x \leq 0.02$) and

eliminate the order for higher concentrations where Δq drops well below 3.0 (e.g., $x = 0.06$, $\Delta q = 2.76$).

The increased Zn:Nb stoichiometry is also responsible for the loss of order in the $(1-x)Ba(Zn_{1/3}Nb_{2/3})O_3$–$xBa(Zn_{1/2}Nb_{1/2})O_{2.75}$ system where the replacement of Nb by Zn is compensated by the formation of oxygen vacancies. In this system, just a small increase in the concentration of Zn ($x = 0.04$) eliminates any evidence for cation order.

For ABO_3-type stoichiometry, solid solutions containing an excess of BaO can be described as $Ba(Ba_xZn_{(1-x)/3}Nb_{(2-2x)/3})O_{3-x}\square_{Ox}$; this formalism is equivalent to representing BaO as $(Ba)_A(Ba)_B(O_2\square_{O1})_{O3}$ in an ABO_3 format. For this description, BZN accommodates the excess BaO by the partial substitution of Ba onto the B site and the introduction of oxygen vacancies. The substitution of the larger Ba cation onto the B sites explains the relatively large expansion in the lattice parameter (Table II) and high-angle peak shifts in the narrow range of stability. The complete loss of 1:2 order in the BaO-excess compositions is also consistent with the incorporation of Ba into the B-site lattice, which reduces Δq and introduces a very large size mismatch between the cations on the ordered sites.

The formation of disordered $(1-x)BZN$–$(x)Ba_4Nb_2O_9$ solid solutions (Fig. 7), which have similar lattice expansions, can be rationalized in a similar way. Here, the barium niobate endmember can be rewritten as $Ba(Ba_{1/3}Nb_{2/3})O_3$; in an ordered solid solution, Ba and Zn would have to occupy the same site and their large size mismatch will severely reduce the driving force for order. The loss of order observed in this pseudo-binary contradicts the original proposal that the volatilization of ZnO and associated increase in order in BZT is due to the replacement of Zn by Ba.[9]

Although an increase in the Zn:Nb ratio precipitates the onset of disorder, the systems where the Zn:Nb ratio is reduced, for example the aforementioned BZN–$Ba_5Nb_4O_{15}$ and BZN–$BaNb_2O_6$ binaries, exhibit the most ordered structures and highest T_{order} observed in the system. The previous discussion of $(1-x)BZN$–$(x)Ba(\square_{1/5}Nb_{4/5})O_3$ focused on the impact of the Zn vacancies on the order; however, these phases, which are stable upto 4% substitution, also contain an excess of niobium and will have an ordered stoichiometry, $Ba[(Zn_{1-x}\square_{3x/5}Nb_{2x/5})_{1/3}Nb_{2/3}]O_3$. While the Zn-excess phases reduce Δq, because Zn is replaced by $(\square_{3/5}Nb_{2/5})$ in this case Δq remains constant. The partial substitution of Nb on the Zn site will still slightly reduce the size difference of the two ordered positions; apparently, this is more than offset by the large destabilization of the disordered phase by the formation of Zn vacancies.

The Zn:Nb ratio is also reduced in the BZN–$BaNb_2O_6$ solid solutions; the range of stoichiometry is narrow (<0.8%) but again they show a large increase in order, a high c/a, and, from additional quenching experiments, an elevated T_{order} ($\sim$1410°C for $x = 0.005$). If $BaNb_2O_6$ is rewritten as $(Ba_{1/2}\square_{Ba1/2})NbO_3$, the ordered solutions can be represented by $(Ba_{1-x/2}\square_{Bax/2})(Zn_{(1-x)}Nb_x)_{1/3}Nb_{2/3}O_3$ with the substitution introducing Ba vacancies as well as additional Nb on the Zn site. Here, the occupancy of Nb on the Zn site does decrease the charge/size difference and yet the ordering is still enhanced. The increase in the relative stability from the Ba vacancies, which are not accompanied by oxygen vacancies, must be sufficient to offset the small reduction in Δq ($= 2.985$ for $x = 0.005$), and the ordered structure is one of the most stable in the system.

The improvement in the order observed in Nb_2O_5-excess BZN is quite surprising. The range of stoichiometry is the smallest observed, <0.5%, and yet the samples again show an enhanced T_{order} ($\sim$1405°C), strong and sharp ordering reflections, and a high c/a. The most likely structural model for this system is one where Nb_2O_5 (or "$(\square_{Ba})NbO_{2.5}\square_{O0.5}$" in perovskite notation) introduces Ba and O vacancies and excess Nb on the Zn site: $(Ba_{1-x}\square_{Bax})[(Zn_{1-x}Nb_x)_{1/3}Nb_{2/3}]O_{3-x/2}\square_{Ox/2}$. The vacancies should increase in the order, but additional Nb would again favor disorder. Because the solubility is so low, it is possible that the excess Nb_2O_5 introduces trace amounts of impurities (e.g., TTB and ZnO) that are not visible in the XRD patterns (or the SEM analyses) and that the composition of the primary perovskite phase actually lies along the BZN–$BaNb_2O_6$ join.

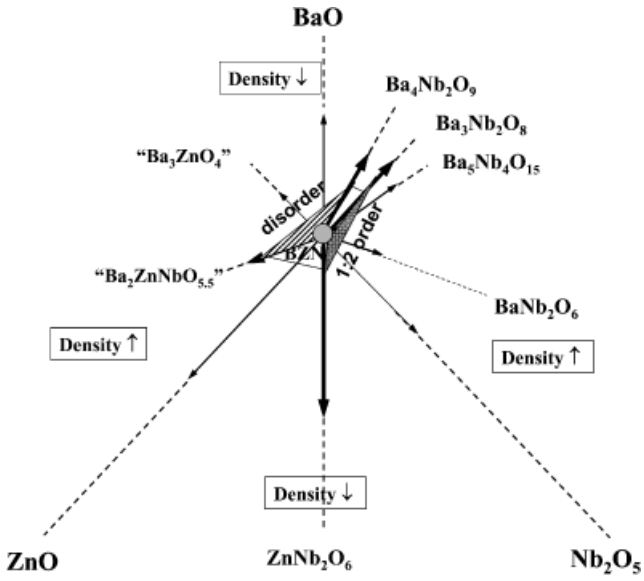

Fig. 20. Summary of the effect of non-stoichiometry on the ordering and sintering properties of $Ba(Zn_{1/3}Nb_{2/3})O_3$ (BZN).

We now turn to the effect of cation non-stoichiometry on the sintering properties and microstructures of BZN ceramics. In addition to their deleterious effect on the cation ordering, the Nb_2O_5-deficient and BaO-excess compositions form porous microstructures with a low density (see Fig. 12). Also, although BaO-deficiency can improve the order, in BZN and BZN–BW, it produces an abrupt decrease in density. These microstructures show exaggerated grain growth, most likely from the enhanced diffusion of the Ba cations. In BaO-deficient BZN–BW, the enhanced diffusion coupled with the formation of a grain boundary liquid phase also produces extensive grain boundary faceting. For all the other directions of non-stoichiometry, the ceramic densities remained high, with small improvements occurring in the $Ba_5Nb_4O_{15}$, $BaNb_2O_6$, and in particular the $Ba(Zn_{1/2}Nb_{1/2})O_{2.75}$ systems; these are summarized in Fig. 12.

The schematic in Fig. 20 summarizes the effect of the small changes in the stoichiometry of BZN on the crystal structure and microstructure that combine to mediate the dielectric loss properties. A distribution map of the resultant $Q \times f$'s after sintering and annealing is presented in Fig. 21. It is clear that the highest $Q \times f$'s ($\sim$110 000) are located in two regions near the $Ba_5Nb_4O_{15}$ and $BaNb_2O_6$ lines; stoichiometric BZN falls in a region where the $Q \times f$ is $\sim$75 000; in the other regions, including excess ZnO, Q decreases rapidly. For BZN, and by analogy,

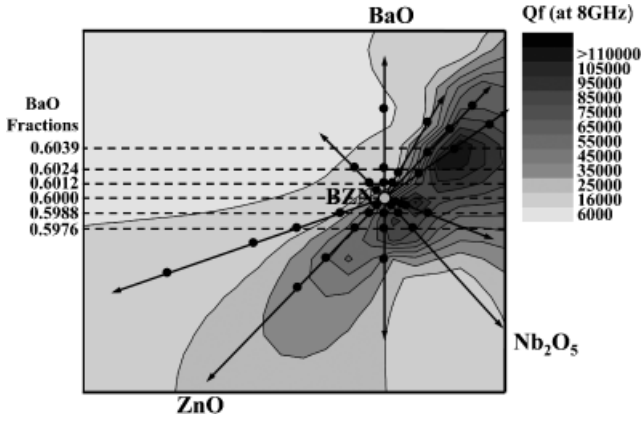

Fig. 21. Map of the variation of $Q \times f$ in the $Ba(Zn_{1/3}Nb_{2/3})O_3$ (BZN) system after sintering and annealing.

possibly all other 1:2 niobate and tantalate microwave perovskites, the highest Q's can be accessed by introducing of small degrees of non-stoichiometry along either the BZN–$BaNb_2O_6$ or BZN–$Ba_5Nb_4O_{15}$ directions. Comparison of the dependence of Q (Fig. 17), c/a (Fig. 11) and relative density (Fig. 12) on the stoichiometry reveals that the changes in Q are directly related to the cation order, given that the ceramics have a reasonably high density ($\sim \geq 95\%$). For example, the order (and c/a) of the BaO-deficient samples along the $ZnNb_2O_6$ line increased systematically with composition; however, the associated increase in Q was only maintained for the lowest substitution, which has a "reasonable" density ($\sim 93\%$), and is then offset by the abrupt decrease in density for the higher compositions where Q was lowered to $<20\,000$. The importance of the ordering is also very evident in the BZN–$Ba(Zn_{1/2}Nb_{1/2})O_{2.75}$ compositions where the relative density increased, but the complete loss of cation order reduced the $Q \times f$ to $\sim 20\,000$. For ZnO-deficient BZN (BZN–$Ba_3Nb_2O_8$), the Q, the cation order, and the density remain essentially constant; for excess ZnO, although the density showed a small increase, the decrease in Q (to $\sim 55\,000$) was clearly associated with the loss of cation order. In the $Ba_4Nb_2O_9$, excess-BaO and excess-Nb_2O_5 (BZN-"Ba_3ZnO_4") directions the precipitous reduction in Q coincides with the loss of order and the large decrease in density. For the three directions showing the highest Q's (excess Nb_2O_5, $BaNb_2O_6$, $Ba_5Nb_4O_{15}$), the density was increased slightly (by a maximum of 1%) compared with stoichiometric BZN; however, c/a increased dramatically, consistent with the large associated increase in Q.

While some papers have claimed that the Q improvements in these systems are primarily associated with changes in density and grain size rather than the cation order, and this can be the case when the ceramics have low densities, our results demonstrate that the cation order dominates the response for high-density ceramics. These results may also explain the large variations in $Q \times f$ reported for BZN, as slightly different starting stoichiometries, or small losses of a component during processing, can yield very different Q's. They may also explain some of the changes observed from the volatilization of ZnO at high temperature. For a very small deficiency of ZnO, the samples can remain single phase and follow a direction toward $Ba_3Nb_2O_8$ where Q remains close to 70 000; for larger losses, the samples will enter a three-phase region that could comprise a primary perovskite phase with a composition along the high Q $Ba_5Nb_4O_{15}$ or $BaNb_2O_6$ lines plus additional impurity phases of $Ba_5Nb_4O_{15}$ (or the eight layer $Ba_8ZnNb_6O_{24}$ phase) and perhaps one other barium niobate phase (e.g., $Ba_4Nb_2O_9$). If the loss of ZnO is not uniform throughout the sample, for example higher in the near-surface regions of the pellets, non-equilibrium assemblages of stoichiometric and non-stoichiometric perovskites would be expected. These could have different degrees of cation order and slightly different lattice parameters and c/a's; this possibility is consistent with the results of Beiringer *et al.*,[8] who observed these types of heterogeneities in their high-temperature diffraction studies of BZT.

The results of this study could also explain the large variations in the properties reported for BZN and BZT after muffling in ZnO-rich atmospheres. In all of our work, the samples were muffled in "sacrificial powders" of the same composition to inhibit the volatilization of ZnO and to avoid any changes in bulk composition. In many other research studies, and in some commercial preparations, ZnO is used as a muffling agent. While ZnO can certainly be effective in inhibiting the loss of ZnO from BZN and avoiding extensive decomposition at high temperature, it is possible that rather than preventing volatilization, the muffling could lead to the formation of ZnO-excess BZN solid solutions either during sintering or during the cooling and subsequent annealing. If this was the case, our $Q \times f$ maps indicate that the properties would deteriorate due to the loss of cation order. The reports on the lowering of Q in ZnO-muffled environments provide support for this argument. We propose that the sensitivity of $Q \times f$ to the loss or gain of ZnO could be minimized by using a non-stoichiometric starting composition that lies within the high $Q \times f$ "plateau" close to the $Ba_5Nb_4O_{15}$ binary. In addition to having a very high Q, if the stoichiometry was changed through the gain or loss of ZnO from the muffling agent, the composition would remain in a region of high Q. This possibility is explored in a subsequent paper.

V. Conclusions

Ten pseudo-binary systems in BaO–ZnO–Nb_2O_5 ternary were studied to examine the extent of any nonstoichiometry in $Ba(Zn_{1/3}Nb_{2/3})O_3$. BZN was found to support a limited range of non-stoichiometry in several directions. Although the non-stoichiometry is very limited (typically 1% or less) in most cases, it is accompanied by small but detectable changes in the unit cell parameters and has a very large impact on the extent and the stability of B-site order, the sintering and microstructure, and the microwave dielectric loss properties. A map of the $Q \times f$'s for the non-stoichiometric compositions shows that the highest Q's do not coincide with a stoichiometric bulk chemistry with Ba:Zn:Nb = 3:1:2. The highest $Q \times f$'s ($\sim 110\,000$ at 8 GHz) are located in two regions near the $Ba_5Nb_4O_{15}$ and $BaNb_2O_6$ lines. Comparison of the dependence of Q, cation order, and density on the stoichiometry indicates that the changes in the loss properties in dense ceramics are dominated by the alterations in the cation order.

References

[1]H. Wu and P. K. Davies, "Influence of Non-Stoichiometry on the Structure and Properties of $Ba(Zn_{1/3}Nb_{2/3})O_3$ Microwave Dielectrics: I. Substitution of $Ba_3W_2O_9$," *J. Am. Ceram. Soc.*, **89** [7] 2239–49 (2006).

[2]K. P. Surendran, M. T. Sebastian, P. Mohanan, R. L. Moreira, and A. Dias, "Effect of Nonstoichiometry on the Structure and Microwave Dielectric Properties of $Ba(Mg_{0.33}Ta_{0.67})O_3$," *Chem. Mater.*, **17**, 142–51 (2005).

[3]C.-H. Lu and C.-C. Tsai, "Reaction Kinetics, Sintering Characteristics, and Ordering Behavior of Microwave Dielectrics: Barium Magnesium Tantalate," *J. Mater. Res.*, **11** [5] 1219–27 (1996).

[4]J. H. Paik, S. Nahm, J. D. Bylin, M. H. Kim, and H. J. Lee, "The Effect of Mg Deficiency on the Microwave Dielectric Properties of $Ba(Mg_{1/3}Nb_{2/3})O_3$ Ceramics," *J. Mater. Sci. Lett.*, **17**, 1777–80 (1998).

[5]I.-T. Kim, K. S. Hong, and S.-J. Yoon, "Effects of Non-Stoichiometry and Chemical Inhomogeneity on the Order–Disorder Phase Formation in the Complex Perovskite Compounds, $Ba(Ni_{1/3}Nb_{2/3})O_3$ and $Ba(Zn_{1/3}Nb_{2/3})O_3$," *J. Mater. Sci.*, **30**, 514–21 (1995).

[6]J. M. Millet, R. S. Roth, L. D. Ettlinger, and H. S. Parker, "Phase Equilibria and Crystal Chemistry in the Ternary System BaO–TiO_2–Nb_2O_5, I," *J. Solid State Chem.*, **67**, 259–70 (1987).

[7]S. M. Moussa, R. M. Ibberson, M. Bieringer, A. N. Fitch, and M. R. Rosseinsky, "In Situ Measurement of Cation Order and Domain Growth in an Electroceramic," *Chem. Mater.*, **15**, 2527–33 (2003).

[8]M. Bieringer, S. M. Moussa, L. D. Noailles, A. Burrows, C. J. Kiely, M. J. Rosseinsky, and R. M. Ibberson, "Cation Ordering, Domain Growth, and Zinc Loss in the Microwave Dielectric Oxide $Ba_3ZnTa_2O_{9-\delta}$," *Chem. Mater.*, **15**, 586–97 (2003).

[9]S. B. Desu and H. M. O'Bryan, "Microwave Loss Quality of $Ba(Zn_{1/3}Ta_{2/3})O_3$ Ceramics," *J. Am. Ceram. Soc.*, **68** [10] 546–51 (1985).

[10]S. Kawashima, M. Nishida, I. Ueda, and H. Ouchi, "$Ba(Zn_{1/3}Ta_{2/3})O_3$ Ceramics with Low Dielectric Loss at Microwave Frequencies," *J. Am. Ceram. Soc.*, **66** [6] 421–3 (1983).

[11]J.-K. Park, D.-Y. Kim, and N.-M. Hwang, "Effect of Excess BaO and Nb_2O_5 on the Grain Coarsening of $Ba(Ni_{1/3}Nb_{2/3})O_3$ Ceramics," *Scripta Mater.*, **44**, 195–9 (2001).

[12]S.-Y. Noh, M.-J. Yoo, S. Nahm, C.-H. Choi, H.-M. Park, and H.-J. Lee, "Effect of Structural Changes on the Microwave Dielectric Properties of $Ba(Zn_{1/3}Nb_{2/3})O_3$ Ceramics," *Jpn. J. Appl. Phys.*, **41** [5A] 2978–81 (2002).

[13]J.-I. Yang, S. Nahm, C.-H. Choi, H.-J. Lee, J-C. Kim, and H.-M. Park, "Effect of Ga_2O_3 on Microstructure and Microwave Dielectric Properties of $Ba(Zn_{1/3}Ta_{2/3})O_3$ Cceramics," *Jpn. J. Appl. Phys.*, **41** [4A] 702–6 (2002).

[14]J.-I. Yang, S. Nahm, C.-H. Choi, H.-J. Lee, and H.-M. Park, "Microstructure and Microwave Dielectric Properties of $Ba(Zn_{1/3}Ta_{2/3})O_3$ Ceramics with ZrO_2 Addition," *J. Am. Ceram. Soc.*, **85** [1] 165–8 (2002).

[15]M.-H. Kim, S. Nahm, W.-S. Lee, M.-J. Yoo, J.-C. Park, and H.-J. Lee, "Effect of Microstructure and Microwave Dielectric Properties of Al_2O_3-Added $Ba(Zn_{1/3}Ta_{2/3})O_3$ Ceramics," *Jpn. J. Appl. Phys.*, **43** [4A] 1438–41 (2004).

[16]V. Tolmer and G. Desgardin, "Low-Temperature Sintering and Influence of the Process on the Dielectric Properties of $Ba(Zn_{1/3}Ta_{2/3})O_3$," *J. Am. Ceram. Soc.*, **80** [8] 1981–97 (1997).

[17]P. K. Davies, A. Borisevich, and M. Thirumal, "Communicating with Wireless Perovskites: Cation Order and Zinc Volatilization," *J. Eur. Ceram. Soc.*, **23**, 2461–6 (2003).

[18]S. M. Moussa, J. B. Claridge, M. J. Rosseinsky, and S. Clarke, "$Ba_8ZnTa_6O_{24}$: A High-Q Microwave Dielectric from a Potentially Diverse Homologous Series," *Appl. Phys. Lett.*, **82** [25] 4537–9 (2003).

[19]A. J. Jacobson, B. M. Collins, and B. E. F. Fender, "A Powder Neutron and X-Ray Diffraction Determination of the Structure of $Ba_3ZnTa_2O_9$: A Investigation of Perovskite Phases in the System Ba–Ta–Zn–O and the Preparation of $Ba_2TaCdO_{5.5}$ and $Ba_2CeInO_{5.5}$," *Acta Cryst.*, **B32**, 1083–7 (1976).

[20]D. Yoon, "Chemically Induced Interface Migration in Solids," *Annu. Rev. Mater. Sci.*, **19**, 43–58 (1989).

[21]S.-J. L. Kang, "Part III Grain Growth, Chapter 8 Interface Migration under Chemical Inequilibrium"; pp. 105–12 in *Sintering*. Elsevier Butterworth-Heinemann, Oxford, 2005.

[22]S. Kawashima, "Influence of ZnO Evaporation on Microwave Dielectric Loss and Sinterability of $Ba(Zn_{1/3}Ta_{2/3})O_3$ Ceramics," *Am. Ceram. Soc. Bull.*, **72**, 120–6 (1993).

[23]M. Abe and K. Uchino, "X-Ray Study of the Deficient Perovskite $La_{2/3}TiO_3$," *Mat. Res. Bull.*, **9**, 147–56 (1974).

[24]M. A. Alario-Franco, I. E. Grey, J. C. Joubert, H. Vincent, and M. Labeau, "Structural Studies on A-Cation-Deficient Perovskite-Related Phases. I. $ThNb_4O_{12}$. Thorium/Vacancy Ordering in Slow-Cooled Samples," *Acta Cryst.*, **A38**, 177–86 (1982).

[25]M. Labeau, I. E. Grey, J. C. Joubert, H. Vincent, and M. A. Alario-Franco, "Structural Studies on A-Cation-Deficient Perovskite-Related Phases. II. Microdomain Formation in $ThNb_4O_{12}$," *Acta Cryst.*, **A38**, 753–61 (1982).

[26]A. R. Chakhmouradian, R. H. Mitchell, and P. C. Burns, "The A-site Deficient Order Perovskite $Th_{0.25}\square_{0.75}NbO_3$: A Re-Investigation," *J. Alloys Compd.*, **307**, 149–56 (2000).

[27]H. Wu and P. K. Davies, "Non-Stoichiometric 1:2 Ordered Perovskites in the $Ba(Li_{1/4}Nb_{3/4})O_3$–$Ba(Li_{2/5}W_{3/5})O_3$ System," *J. Solid State Chem.*, **177** [10] 3469–78 (2004).

[28]H. Wu and P. K. Davies, "Ordered Perovskites in the $A^{2+}(Li_{1/4}Nb_{3/4})O_3$–$A^{2+}(Li_{2/5}W_{3/5})O_3$($A^{2+}$ = Sr, Ca) Systems," *J. Solid State Chem.*, **177** [11] 4305–1 (2004).

[29]M. A. Akbas and P. K. Davies, "Cation Ordering Transformations in $Ba(Zn_{1/3}Nb_{2/3})O_3$–$La(Zn_{2/3}Nb_{1/3})O_3$ System," *J. Am. Ceram. Soc.*, **81** [4] 1061–4 (1998). □